Fall 2016

Field induced assembly of particulate systems

Kinnari Shah
New Jersey Institute of Technology

Copyright Warning & Restrictions

The copyright law of the United States (Title 17, United States Code) governs the making of photocopies or other reproductions of copyrighted material.

Under certain conditions specified in the law, libraries and archives are authorized to furnish a photocopy or other reproduction. One of these specified conditions is that the photocopy or reproduction is not to be "used for any purpose other than private study, scholarship, or research." If a, user makes a request for, or later uses, a photocopy or reproduction for purposes in excess of "fair use" that user may be liable for copyright infringement,

This institution reserves the right to refuse to accept a copying order if, in its judgment, fulfillment of the order would involve violation of copyright law.

Please Note: The author retains the copyright while the New Jersey Institute of Technology reserves the right to distribute this thesis or dissertation

Printing note: If you do not wish to print this page, then select "Pages from: first page # to: last page #" on the print dialog screen

ABSTRACT

FIELD INDUCED ASSEMBLY OF PARTICULATE SYSTEMS

by
Kinnari Shah

The primary focus of the first part of this dissertation is to study the AC field-driven assembly of monodisperse silica and glass particles on liquid - liquid interface and forming a liquid film of uniform thickness having arrangement of particles on it. This liquid film with arrangement of regular particles can be converted into a solid film by curing top UV curable liquid. Here, electric field is used as a tool to facilitate AC field-driven assembly. The work describes the assembly of different size of regular particles and effective development of solid film.

It is also shown that particles of two dissimilar sizes and dielectric properties can be assembled on Air-liquid interface and form assembly of dual particles with ring structure. In this work, two dissimilar particles are trapped between an interface and AC electric field is applied to particle suspensions in a gap between the top and bottom electrodes. In order to exploit the concept of dual particle assembly, mixture of glass particles and plastic latex particles are studied. It is noticeable that the lateral dipolar force leads two particles to either repel or attract. This force of repulsion and attraction between particles depend on their polarizabilities and the intensity of the force. Finally, rapid and effective formation of ring structure of dual particles is shown. The study is also extended for mixture of particles that are less than 10 μm. In all cases, it is observed that smaller

particles act as the binder for larger particles and form dual particle ring structure since they have a reverse polarizability.

In the third part of this dissertation, AC electric field is used to assemble the particles on the freely suspended single floating droplet on immiscible liquid. Particles on the droplet can be levitated and assembled at the pole or equator due to dielectric properties and conductivity of particles and liquid medium when low frequency is applied. Under high frequency, particles drag towards the pole or equator due to Clausius Mossotti factor of particle and droplet. The high and low frequency are distinguished by crossover frequency. Here, crossover frequency is investigated experimentally and assembly of the different particles at the pole or equator of the droplet is shown. At any initial location of the particle and considering the very low frequency, flow deceases with increase in frequency - this is studied experimentally.

A diffusing particle is subjected to a variety of collisions that leads to a random or Brownian motion. Assembly of particles of various sizes with various viscous media are studied in the first and second part. It is experimentally observed that Brownian motion decreases with increase in particle size. The aim of this study is to highlight the visualization of Brownian motion and compute the transmission probability from inner to outer region under the conditions of varying viscosity, particle size and temperature. The obtained results are validated with Stokes-Einstein equation and Fang and Ning's experimental and theoretical work. It is shown that the transmission probability increases with decrease in viscosity and particle size and increase in temperature.

FIELD INDUCED ASSEMBLY OF PARTICULATE SYSTEMS

by
Kinnari Shah

A Dissertation
Submitted to the Faculty of
New Jersey Institute of Technology
in Partial Fulfillment of the Requirements for the Degree of
Doctor of Philosophy in Mechanical Engineering

Department of Mechanical and Industrial Engineering

January 2017

.

APPROVAL PAGE

FIELD INDUCED ASSEMBLY OF PARTICULATE SYSTEMS

Kinnari Shah

Dr. N. M. Ravindra, Dissertation Co-Advisor — Date
Professor of Physics/Interdisciplinary Program in Material Science and Engineering
New Jersey Institute of Technology

Dr. I. Joga Rao, Dissertation Co-Advisor — Date
Professor and Chair of Department of Mechanical and Industrial Engineering
New Jersey Institute of Technology

Dr. Siva P. Nadimpalli, Committee Member — Date
Assistant Professor of Mechanical and Industrial Engineering
New Jersey Institute of Technology

Dr. Eon Soo Lee, Committee Member — Date
Assistant Professor of Mechanical and Industrial Engineering
New Jersey Institute of Technology

Dr. Michael Jaffe, Committee Member — Date
Research Professor of Biomedical Engineering
New Jersey Institute of Technology

BIOGRAPHICAL SKETCH

Author: Kinnari Shah

Degree: Doctor of Philosophy

Date: January 2017

Undergraduate and Graduate Education:

- Doctor of Philosophy in Mechanical Engineering,
  New Jersey Institute of Technology, Newark, NJ, 2017.

- Master of Science in Mechanical Engineering
  Stevens Institute of Technology, Hoboken, NJ, 2010

- Master of Engineering in Turbomachine
  S V National Institute of Technology, Surat, India

- Bachelor of Engineering in Mechanical Engineering
  Sardar Patel University, Anand, India

Major: Mechanical Engineering

Presentations and Publications:

K. Shah and R. Nuggehalli, "Transmission Probability of Diffusing Particles – A Case Study," TMS 2017 146th Annual Meeting and Exhibition on Recent Developments in Biological, Structural and Functional Thin Films and Coatings, San Diego, California February-March 2017.

E. Amah, K. Shah, I. Fischer and P. Singh, "Electrohydrodynamic Manipulation of Particles Adsorbed on The Surface of a Drop," Soft Matter, 12, 1663-1673, 2016.

E. Amah, K. Shah, I. Fischer and P. Singh, "Electrohydrodynamic Manipulation of Particles Adsorbed on the Surface of a Drop," 68th Annual Meeting of the APS Division of Fluid Dynamics, Boston, Massachusetts, November 2015.

P. Singh, M. Hossain, S. K. Gurupatham, K. Shah, E. Amah, D. Ju, M. Janjua, S. Nudurupati and I. Fischer, "Molecular-like Hierarchical Self-assembly of Monolayers of Mixtures of Particles," Nature Scientific Reports 4, 7427, 2014.

E. Amah, K. Shah, I. Fischer and P. Singh, "Electrohydrodynamic Manipulation of Particles on The Drop Surfaces," 67th Annual Meeting of the APS Division of Fluid Dynamics, San Francisco, California, November 2014.

K. Shah, M. Hossain, M. Janjua, N. Aubry, I. Fischer and P. Singh, "Electric Field Induced Self-assembly of Monolayers of Sub-micron Sized Particles on Flexible Thin Films," Society of Rheology 86th Annual meeting, Philadelphia, Pennsylvania, October 2014.

K. Shah, E. Amah, I. Fisher and P. Singh, "Concentration and Separation of Particles Adsorbed on The Drop Surface," Graduate Research Showcase, New Jersey Institute of Technology, NJ, October 2014.

E. Amah, K. Shah, I. Fischer and P. Singh, Self-assembly and Manipulation of Particles on Drop Surfaces, ASME 2014 4th Joint US-European Fluids Engineering Division Summer Meeting (FEDSM' 14-21792) Chicago, Illinois, August 2014.

K. Shah, M. Hossain, E. Amah, I.S. Fischer and P. Singh, "Electric Field Induced Self-assembly of Monolayers of Sub-micron Sized Particles on Flexible Thin Films," Female Research Showcase 2014, Society of Women engineering, New Jersey Institute of technology, NJ, March 2014.

K. Shah, M. Hossain, M. Janjua, N. Aubry, I. Fischer and P. Singh, "Electric Field Induced Self-assembly of Monolayers of Sub-micron Sized Particles on Flexible Thin Films," 66th Annual Meeting of the APS Division of Fluid Dynamics, Pittsburgh, Pennsylvania, November 2013.

K. Shah, M. Hossain, M. Janjua, N. Aubry, I. Fischer and P. Singh, "Electric Field Induced Self-assembly of Monolayers of Sub-micron Sized Particles on Flexible Thin Films," Graduate Research Showcase, New Jersey Institute of Technology, NJ, October 2013.

M. Hossain, K. Shah, D. Jhu, S. Gurupatham, I. Fischer, N. Musunuri and P. Singh, "Self-assembly of Monolayers of Micron Sized Particles on Thin Liquid Films," ASME 2013 Fluid Engineering Division Summer Meeting (FEDSM'13-16271), Incline Village, Nevada, July 2013.

This work is dedicated to

My son: Aagam and my husband: Sunil who have been with me through thick and thin. My mother: Hemlata for her unconditional love and my sister: Namrata for her care and advice in each step I follow

ACKNOWLEDGMENT

First and foremost, I convey my deepest gratitude to Dr. N. M. Ravindra (Dr. Ravi) for agreeing to be my dissertation advisor. His valuable knowledge, timely help and his dedication towards the subject matter led me to complete my research. He has been a constant motivator right for me from the day when I took his class and still continues to be. I strongly respect his valuable support and co-operation during my difficult personal times. He is very kind and the most noticeable is the way he treats students. Although our relationship as student/advisor ends here, I am certain and look forward to him always as being my mentor. My heartiest thanks to Dr. Ravi.

My very sincere thanks to Chair of Mechanical and Industrial Engineering Department and advisor Dr. I. Joga Rao. I appreciate his timely help and gentle advice which made a difference during my difficult and pleasant times. I took his course 'Continuum mechanics' which is a very tough course but the way he taught this course became very interesting and thorough.

It has been my privilege to benefit from Dr. Ravi and Dr. Rao's patience, kindness and a genuine interest in my welfare.

I convey my great thanks to Dr. Siva P. Nadimpalli, Dr. Eon Soo Lee, and Dr. Michael Jaffe for the time they each took out of their busy schedules to provide me a fresh perspective in my work.

My gratitude is also extended to Mr. David, Ms. Clarisa González-Lenahan and Dr. Sotirios G. Ziavras for their minute observations and help in organizing the write up.

How can I forget Dr. Harnoy Avraham for his advice and compliments while communicating with him. I am so much thankful to him. I am also thankful to Prof. Balraj Mani, Dr. Swapnil Moon, Dr. Herli Surjanhata, and Dr. Samardzic Veljko for their direction while performing my teaching assignment.

I would like to thank the administrative staff of Mechanical and Industrial Engineering department - Ms. Barbara Jean Valenti, Ms. Aileen Checa, Ms. Yvonne Williams, and SWE coordinator Ms. Lucie T. Tchouassi. I am also thankful to Mr. Joseph Glaz and Mr. Gregory Policastro for their co-operation while conducting the laboratory.

I would like to acknowledge the Mechanical and Industrial Engineering Department, New Jersey Institute of Technology for providing me financial support throughout my doctoral study.

I would like to thank my friends and relatives who directly or indirectly supported me during my Ph. D Study.

Very important, I am thankful to my son Aagam, , husband Sunil, mother Hemlata, my sister Namrata and her family, my brother for their love and affection. My father provided his counsel throughout my life and career and was always ready to take my responsibilities on him even today. I wish him healthy life. I greatly appreciate the co-operation of my mother in-law Pravinaben and father in–law Subhashbhai throughout my study.

Last but not the least, I am thankful to GOD for the strength for doing hard work and dedicating myself to every task I performed.

TABLE OF CONTENTS

Chapter		Page
1	GENERAL INTRODUCTION……...	1
	1.1 Forces in Colloidal Suspensions……	2
	1.2 Major Types of Field Assisted Manipulations……	5
	1.3 Surface Science and Assembly……..	13
	1.4 Research Objective……	16
2	FIELD INDUCED ASSEMBLY OF MONODISPERSE PARTICLES……	19
	2.1 Overview……..	19
	2.2 Governing Equations……	19
	2.3 Material Property and Experimental Setup…….	22
	2.4 Results and Discussion…….	24
	2.4.1 Solid Film with Assembled 20 μm Glass Particles……..	26
	2.4.2 Solid Film with Assembled 45 μm Glass Particles……...	27
	2.4.3 Assembly of Silica Particles less than 5 μm……..	28
	2.4.3.1 Development of Solid Film with Assembled 2.25 μm Silica Particles…….	29

2.4.3.2 Assembly of 480 nm Silica Particles on Corn Oil-Adhesive Interface…….. 32

3 FIELD INDUCED ASSEMBLY OF DUAL PARTICLES……... 33

3.1 Overview……... 33

3.2 Governing Equations…… 33

3.3 Material Properties…….. 34

3.4 Results and Discussion…… 35

3.4.1 Ring Structure of 20 µm Glass Particles and 71 µm Copolymer Latex on The Surface of Silicone Oil……... 36

3.4.2 Ring Structure of 20 µm glass particles and 71µm copolymer latex on The Surface of Hallbrite Oil…… 38

3.4.3 Ring Structure of 8 µm Glass Particles and 4 µm Polystyrene Latex on the Surface of Adhesive……. 39

4 FIELD INDUCED ASSEMBLY OF PARTICLES INSIDE THE DROPLET…… 41

4.1 Overview…… 41

4.2 Theoretical Background……. 42

4.3 Material Properties and Methodology…… 43

4.4 Results and Discussion…… 44

4.4.1 Effect of AC Electrohydrodynamic Force at Very Low Frequency…….. 44

4.4.2 Assembly of Particles at Pole or Equator of a Droplet…….. 48

4.4.3 Sorting out the Hollow Glass Sphere and Solid Particles from The Mixture ..51

5 TRANSMISSION PROBABILITY OF DIFFUSSING PARTICLES: A CASE STUDY 53

5.1 Overview…… 53

5.2 Theoretical Background……. 53

5.3 Methodology…….. 55

5.4 Results and Discussion……... 56

5.4.1 Transmission Probability and Visualization of Brownian motion at Various Temperature…… 58

5.4.2 Transmission Probability and Visualization of Brownian motion at Various Viscosity……. 59

5.4.3 Transmission Probability and Visualization of Brownian motion at Various Particle Size…… 60

6 CONCLUSION……... 62

7 APPLICATIONS…… 64

8 SCOPE OF FUTURE WORK…… 65

REFERENCES…… 66

LIST OF TABLES

Table **Page**

1.1 Summary of Electrokinetic Forces Exerted on Particles

2.1 Properties of Particles -I

2.2 Properties of Fluids-I

3.1 Properties of Particles-II

3.2 Properties of Fluids-II

4.1 Various Calculated Factors for Various Case

4.2 Properties of Particles-III

4.3 Properties of Fluids-III

LIST OF FIGURES

Figure **Page**

1.1 AC Dielectrophoretic manipulation techniques: electroporation (a), electro-orientation (b), particle trapping (c), and traveling wave dielectrophoresis (d) .

2.1 Heavy solid spherical particle in equilibrium at oil-water interface

2.2 Schematic diagram of the experimental setup

2.3 Initial image of 20 μm particles under capillary force 200X magnification (a), Particle influence by electric field and started arranging (b), self-assembled and arranged 20 μm particle on two liquid interface before freezing at 200X magnification after electric field applied (c), Microscopic view of flexible solid film with 20 μm particles after curing/freezing 500x magification (d).

2.4 Initial image of 45μm glass particles 50X magnification (a), Arranged 45 μm particles on two liquid interfaces on 200X magnification after electric field applied (b)

2.5 Microscopic view of flexible solid film with 45 μm particles after curing/freezing 500X magification (c) and (d)

2.6 2.25 μm particles on solid film showing that arrangement got disturbed after freezing (a), Scanning Electron Microscopy (SEM) image of 2.25 μm particles with irregular arrangement on solid film (b).

2.7 Initial image of 2.25 μm particle (a), 2.25 μm particles influenced by electric field (b), Solid film of 2.25 μm silica particles after freezing (c), Microscopic view of solid film which has 2.25 μm particles arranged on it (d).

2.8 480nm silica particles on 500X magnification before electric field applied on adhesive-corn oil interface (a), particles got arrangement after electric field applied at 500X magnification (b).

3.1 Monolayers of dual particle ring structure of 71 μm copolymer and 20 μm glass particles on the surface of silicone oil. Initial distribution of both particles 50X (a), After electric field was applied (500X) (b).

3.2 Assembly of dual particle ring structure of 71μm copolymer and 20 μm glass particles on the surface of Hallbrite oil after applying electric field (500X) (a) and (b).

3.3 Monolayers of dual particles ring structure of 8μm glass particles and 4μm Polystyrene particle on Air –Adhesive interface. The magnification is 200X. Initial distribution of both particles (a), After electric field was applied, the mixture self-assembled to form composite particles (b), (c), (d)

4.1 Effect of frequency on Electrohydrodynamic flow of 1-3 μm Solid glass particles Initial Image (a), Droplet at 0.1 Hz frequency (b), Droplet at 0.2 Hz frequency (c)

4.2 Effect of frequency on Electrohydrodynamic flow of 1-3 μm Solid glass particles Initial Image with particles concentrated at pole (a), Droplet at 1 Hz frequency (b), Droplet at 1.4 Hz frequency (c), and droplet at 1.8Hz frequency (d)

4.3 Effect of frequency on Electrohydrodynamic flow of 1-3 μm Solid glass particles droplet at 0.25 Hz (a), Droplet at 0.4 Hz frequency (b)

4.4 Initial Image of silicone oil droplet contained hollow glass particles on the castor oil medium (a), At 0.1Hz particles at Pole (b) and At 0.1Hz particles at Pole (c)

4.5 Initial Image of silicone oil droplet contained Solid glass particles on the castor oil medium (a), At low frequency particles at Pole (b), and at high frequency particles at Pole (c)

4.6 Initial Image of silicone oil droplet contained Polystyrene on the castor oil medium (a), Particles at Pole at 6 Hz (b) and Particles diverting towards equator at 12 Hz (c)

4.7 Initial Particles of mixture of particles (a), Solid glass particles at pole and Hollow glass particles at equator at 6 Hz (b)

5.1 Transmission probability at different temperature (a), the computed transmission probability 300K (b), and the computed transmission probability 450K (c)

5.2 Transmission probability at varying viscosity

5.3 Transmission Probability at varying particle size.

CHAPTER 1

GENERAL INTRODUCTION

For many years, the study of colloidal systems has proved to be a very valuable and fundamental endeavor both academically and commercially. External Field-directed colloidal assembly has gained attention due to its remarkable recent progress in increasing the complexity, degree of control, and multiscale organization of the structures. Colloidal assembly represents a fascinating phenomenon that can be used as a tool to explore condensed matter physics and fabrication of advanced materials, such as photonic crystals, molecular sieves, and other higher ordered structures which have been recently documented [1-4]. The stability of any colloidal suspension is highly dependent on short range forces, (e.g. Steric, Van der Waals, and depletion); However, due to some dynamic effects, such as long relaxation times, slow diffusion, which are influenced by the larger particle size and also the interparticle interactions of the nanoscale colloidal spheres, they do not assemble themselves into their thermodynamically lowest energy state naturally. In such systems, thermodynamics no longer causes the ordering process or if does only after a very long time as they are far from equilibrium. Therefore, ordering of the particles need to be directed by applying external forces on the systems such as optical, acoustic, gravity, electric or magnetic fields to control long-range interfacial forces by means of physical confinement. For very small particles, gravitational force is negligible.

Dynamic assembly of colloidal nanoparticles depends on various factors, such as the particle interactions, particle size, size distribution, particle shape, surface charge, density, nature and the dimensions of the external forces, substrate surface properties as well as the other environmental factors such as temperature, evaporation rate etc.

1.1 Forces in Colloidal Suspensions

Various forces acting on colloidal suspension are reviewed here. These include the following:

- Van der Walls Forces (Attractive force)
- Double Layer (Electrostatic) (Repulsive force)
- Steric Interactions (Repulsive force)
- Depletion interaction (Attractive Force)

Van der Walls Forces: Colloidal objects in fluids experience different forces. At short range, the strongest interaction forces are collectively referred to as the Van der Waals forces. This is a universal force like gravitational force, which exists between all atoms, molecules and colloidal particles even if they are totally neutral. Generally, these arise due to fluctuations of dipoles. To some extent, these fluctuations are of thermal nature. Quantum mechanical fluctuations, however, also play an important role. London's dispersion force (induced dipole-induced dipole force) is one example of a force between surfaces that arises due to quantum fluctuations of electromagnetic fields. In most situations, Van der Waals forces are attractive. This usually leads to strong aggregation when particles approach each other to a fraction of their diameter. For identical spherical particles, with radius a, and a center to center distance r, the Van der Waals interaction depends on a material constant A and the geometry of the particle; the Van der Waals potential energy, after adding all three types of possible dipole interactions, may be expressed as [5,6]:

$$V_{vdw} = -\frac{A_{121}}{6}\left[\frac{2a^2}{r^2-4a^2} + \frac{2a^2}{(r)^2} + \ln\left(\frac{r^2-4a^2}{(r)^2}\right)\right] \tag{1.1}$$

The Hamaker constant, A_{121} depends on the dielectric properties of the spheres and surrounding medium and can be calculated utilizing the Lifshitz theory [6,7].

Double Layer (Electrostatic): Since Van der Waals forces are mostly attractive, some repulsive interaction forces between particles are needed to maintain relatively stable suspensions. Repulsive forces could be due to variety of sources. In aqueous solutions, these repulsive forces are usually due to the presence of various ionic species. In fact, pure water itself will dissociate into positive and negative ions to some degree. Various molecules that are attached to surfaces of particles will also dissociate in solutions leaving some charged species attached to the particles' surfaces. In some cases, ions in the solution will adsorb onto the particles' surfaces. In all these cases, the particles will acquire some net charge balanced by the charge in the surrounding solution. In fact, the charge in the solution around a particle will distribute itself in such a way that the effect of the charge of the particle will be screened and its electrostatic field will decay exponentially away from the particle. Such an arrangement of charges is called a double-layer since the charge on the particle and charge in the solution are opposite in sign.

When two particles, similarly screened by the charges in the solution, approach each other, the charge density between the particles can exceed the charge density elsewhere in the solution. This leads to particles effectively repelling each other. This repulsive interaction is often called the double-layer interaction. One of the simplest approximations for the potential energy of the double-layer interaction is:

$$U_{dl} = \pi \varepsilon d \psi^2 \ln\left(1 + e^{(-\lambda s)}\right) \tag{1.2}$$

where, Ψ is the potential on the particle surface, λ is called the inverse Debye length which is the characteristic scale over which the charge density around a particle decays, and ε is the permittivity of the dispersion medium.

Steric Interactions: Steric interaction is another category of repulsive interactions. As opposed to double-layer, this type of interaction does not necessarily involve charged species. Instead, steric interaction typically relies on molecules with relatively long tails (such as some polymers) that are attached to the surface of the particle. In solution, the tails of molecules that are attached to the particles are relatively free to move around and gyrate in various ways. When two particles approach each other too closely, the movement of the molecular tails becomes more confined, which results in repulsive forces between particles. Steric interaction can be viewed as the resistance to the confinement of such molecular motions.

Manipulation of colloidal systems [8] is a very complex phenomenon and various factors play role in order to achieve control over it; some of the parameters are as follows:

- Effectiveness: whether all or only a percentage of the particles respond in the expected fashion;
- Time scale: if the response is instantaneous or requires a long time period;
- Scale: single or few particle manipulations versus large-scale processes;
- Resources: whether the materials and equipment are expensive, complex and sensitive versus low-cost and simple;
- Properties: if the particle properties are suitable, for example, magnetic manipulation cannot be used with a particle system that has no magnetic properties;
- Application: high value versus commodity.

1.2 Major Types of Field Assisted Manipulations

This section will describe four major types of field-assisted manipulation techniques namely optical manipulation, acoustic manipulation, electrical manipulation and magnetic manipulation which have the advantage of being shaped through the use of lasers, sonic waves, electrodes, and external coils, respectively. Limitations of route of manipulation technique are also described. The later section will discuss electric manipulation technique which is suitable for both particle-surface and particle-particle assembly which is followed by several results of manipulation of micron (μm) and less than 5 μm size silica particles and copolymer particles in which electric field has been used to assemble the particles. This section will end after a brief introduction of electric manipulation technique, which is the major colloidal manipulation technique used in this proposed research.

Optical Manipulation: Optical manipulation of colloidal particles is achieved with a highly focused laser beam that is used to exert dielectric forces on micro particles [9]. Optical manipulation has high spatial and force resolution. One of the major applications is optical tweezers in the measurement of the mechanical properties of single molecules, membranes, and other soft matter. However, the small forces induced by optical fields (up to hundreds of picoNewtons) and large heat produced by focused laser beams can damage the fragile system, and change the parameter of thermodynamics system. Additionally, this technique requires expensive and bulky setup which prevents it from being widely adopted [10-12].

Acoustic Manipulation: Acoustic manipulation is an emerging particle manipulation technique, which has attracted more and more interest because of its high biocompatibility and wide range of applications [13-14]. In this technique, a resonating piezoelectric

transducer (PZT) is driven at a frequency that matches the device geometry, which results in a resonance condition, known as an acoustic standing wave [15-18]. Compared to other manipulation techniques, acoustic manipulation system is non-invasive, making it suitable for biological applications. It does not require bulky/complicated tools, which makes it suitable for on-chip devices. However, it is hard to manipulate the particles that are smaller than 10 μm by this route.

Magnetic Manipulation: Magnetic manipulation, also known as magnetophoresis, is based on the magnetic interaction between colloidal particles and an external magnetic field. Magnetophoresis is similar to dielectrophoresis in theory as well as applications. Due to the high similarity, magnetic manipulation shares the same advantages as electric manipulation. Additionally, magnetic manipulation has several additional advantages: First, unlike electric manipulation, magnetic manipulation normally uses static or slowly-varying magnetic field, which obviates significant heating of samples or sample damages that are associated with high frequency fields, reduced charging, making it suitable for biological and diagnostic applications. Second, compared to dielectrophoresis, magnetic field is able to exert forces of tens of nanonewtons onto micro particles and hence penetrate deeper into the fluids and cause less fluid flow. This feature makes the control of interactions more remote, more precise and easier to model. Also this technique can be implemented with use of common permanent magnets which makes magnetophoresis set up more economical and mobile, but can be applicable to magnetically active particles.

Electrical Manipulation: Electric manipulation is another powerful and well-developed technique for particle manipulation. It is explored in the present work. Although an external electric field can apply force to both charged and uncharged particles, the force is produced

by different mechanisms. The manipulation of charged particles by an electric field is normally referred to as electrophoresis [19]. The manipulation of uncharged particles in an electric field is referred to as dielectrophoresis [20].

Herbert Pohl coined the term dielectrophoresis and was one of the first to study particle electrokinetics in the 1950s. His work focused particularly on the manipulation of polarizable particles with non-uniform fields [20,21]. The advancement of micro fabrication techniques and the demand for Lab-on-a-Chip technologies have led to the development of dielectrophoresis techniques for particulate, biological, and pharmaceutical applications. Dielectrophoresis was initially used to manipulate particles and cells in the micrometer range (1 mm to 1 mm). It has been known since the discovery in antiquity that electrostatic interactions between objects (such as a rubbed material picking up small items) can induce a force, either attractive or repulsive. Since the early 1990s, nanotechnology has incorporated dielectrophoresis for the manipulation of viruses, DNA, protein molecules, and other nanoparticles (diameters of 1 nm to 1 mm), actuate printers and hence produce the written word, to separate and sequence strands of DNA and hence diagnose diseases, to flip mirrors the size of blood cells and hence make data projectors work. The list is endless. Also, the size of the entity is decreased, so electrostatic interactions become one of the dominant forces acting on the object. This is important, since the manipulation of ever-smaller objects has increasingly become the foundation of technological development.

For most dielectrophoresis cases, the applied electric field is an alternating current (AC) signal, created with a common frequency generator. In typical experimentation, frequencies are generally greater than 100 kHz with magnitudes below 20 V peak to peak.

The shape of the signal is typically sinusoidal, but pulse signals have also been used in dielectrophoresis applications. This signal is applied to electrode geometries and electrodes are typically fabricated on the surface of silicon wafers, glass substrates or ITO coated glass substrates in order to visually see species of interest by optical means. It is possible to manipulate, separate, or group targeted particles, cells, droplets with novel electrode geometry design and fabrication. Due to its simplicity in fabrication and its susceptibility to visual observation and analysis, dielectrophoresis is a favorable technique in the current scenario in academia.

Dielectrophoretic forces, though, can be induced by means other than an applied electric signal through electrodes. Optical tools can be implemented to modify an applied electric field, making these methods more susceptible for dynamic as opposed to static manipulation of electric fields with surface electrodes. Dielectrophoresis applications are not limited to particulate manipulation either. With properly configured surface-electrode geometry, it is possible to induce fluid motion and create nanoliter-sized droplets. Additionally, dielectrophoretic forces can be utilized to manipulate particles to build micro- and nanostructures such as wires.

Dielectrophoresis is the translational motion of a particle by induced polarization in a non-uniform electric field. When conductive, uncharged particles are exposed to an electric field, they will polarize, inducing a dipole on the particle. The magnitude and charge orientation of the induced dipole are dependent on the permittivities and conductivities of the medium and of the particle. If the electric field is uniform, the induced charges on both sides of the particle are equal, creating no net force on the particle. However, if the electric field is non-uniform, there will be a net force greater than zero.

The general expression for the dielectrophoretic force of a homogeneous sphere is expressed as [20,21]:

$$\vec{F}_{DEP} = 2\pi a^3 \varepsilon_m \,\mathrm{Re}\left(\frac{\varepsilon_p - \varepsilon_m}{\varepsilon_p + 2\varepsilon_m}\right)\nabla\left|\vec{E}\right|^2 \tag{1.3}$$

where $\left|\vec{E}\right|$ is the electric field, a is particle radius, ε_m is the electric permittivity of the medium, and ε_p is the electric permittivity of the particle. ε_m and ε_p are complex numbers that are dependent on the frequency of the external field. The factor $\left(\frac{\varepsilon_p - \varepsilon_m}{\varepsilon_p + 2\varepsilon_m}\right)$, defined as Clausius-Mossotti factor, determines the effect of the dielectric force. *Re* means the real part of Clausius-Mossotti factor. The Clausius-Mossotti factor is a function of frequency, and, depending on the dielectric properties of the medium and the particle, this factor can be either positive or negative with a possible range of +1.0 to - 0.5. When the real part of Clasius-Mossotti factor is positive or in other words, the dielectric constant of the particle ε_p is larger than that of the surrounding medium, ε_m, *i.e.* the particle is more polarizable than the fluid, the dielectric force pushes the particle towards electric field maximum, and the phenomenon is referred to as positive dielectrophoresis [20, 21].

When the real part of Clausius-Mossotti factor is negative or in other words, the dielectric constant of the particle ε_p is smaller than that of the surrounding medium, ε_m,, *i.e.* the particle is less polarizable than the medium, the dielectric force pushes the particle towards the electric field minimum, and the phenomenon is referred to as negative dielectrophoresis [20,21].

The majority of dielectrophoretic manipulation of particles includes translating (dielectrophoresis), rotating (electrorotation), orienting (electro-orientation), trapping, and using traveling wave dielectrophoresis which is shown in Figure 1.1 [22].

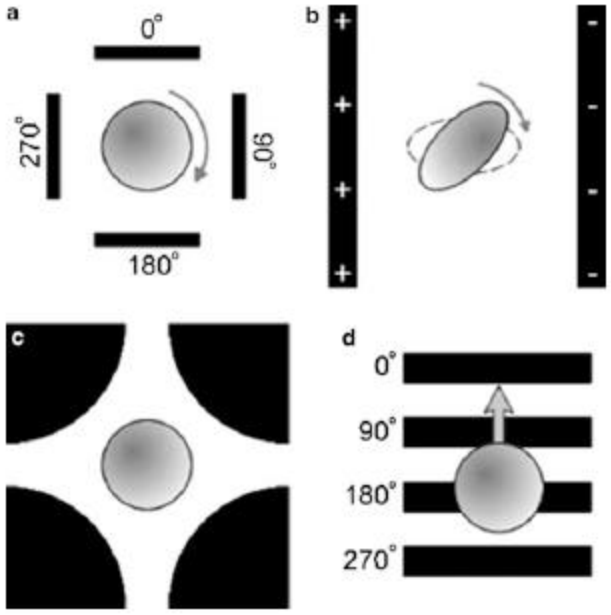

Figure 1.1 AC Dielectrophoretic manipulation techniques: (a) electrorotation, (b) electro-orientation, (c) particle trapping, and (d) traveling wave dielectrophoresis. *Source: [22]*.

Table 1.1 Summary of electrokinetic forces exerted on particles. *Source: [23]*

Force	AC OR DC	Origin
Electrophoresis	DC	Caused by charge in electric field
Dielectrophoresis	AC/DC	Caused by Induced dipole in non-uniform field
Electro-osmosis	AC/DC	Caused by interaction between free charge in electric double layer and tangential electric fields
Electrorotation	AC	Caused by dipole lag in rotating electric field
Travelling wave dielectrophoresis	AC	Caused by dipole lag in travelling electric field
Electro-orientation	AC/DC	Caused by interaction between dipole and electric field

Figure 1.1 provides an illustrative representation of each technique and Table 1.1 summarizes all the techniques which are collectively referred to as AC (alternating current) electrokinetics. In electro rotation, a torque is applied to a particle that is subjected to a rotating electric field (Figure 1.1a). The induced dipole takes a finite amount of time to polarize in a neutral dielectric particle, which attempts to orient itself with the direction of the electric field. This dipole, though, lags behind the applied rotating electric field. The reorientation of the dipole with the electric field induces a torque on the particle, rotating it. Next, electro-orientation involves the alignment of a non-spherical particle in a uniform electric field (Figure 1.1b). When an ellipsoidal particle polarizes, the dipole moment will align the particle with its longest nondispersed dipole parallel to the field lines. Its orientation is a function of the electric field frequency and the dielectric properties of the medium and the particle. Dielectrophoretic forces, though, can be used to not only rotate a particle, but trap it as well. There are two types of particle trapping, those that utilize pDEP or nDEP forces. For example, four electrodes can be positioned in a quadrupole arrangement and, when the appropriate electric field is applied, a particle or particles that are trapped in the electric field null at its center (Figure 1.1c). Traveling wave dielectrophoresis is the linear application of electrorotation (Figure 1.1d). An AC electric wave is produced by applying an electric field that travels linearly along a series of electrodes. The particle will translate in the same or opposite direction as the traveling wave depending on the properties of the applied signal frequency and the dielectrics of the particle and medium [23-25].

In the present work, Dielectrophoresis is utilized in assembly procedures to induce particle-particle interactions or to use attractive forces between electrodes to position a

component and complete a circuit. When two polarized particles come into close proximity to each other, they will undergo an attractive force due to their dipole interactions. This is referred to as dipole-dipole interaction, mutual dielectrophoresis, or pearl chaining because this phenomenon creates strings of particles [26-28]. Recall that a particle's induced dipole aligns itself to the electric field and that like particles will always have the same dipole orientation. These particles will have an attractive force since their opposite charges are aligned facing each other. Additionally, these particle chain formations can also be attributed to the distorted electric field caused by the particle's induced dipole. These field disturbances can cause a localized dielectrophoretic force, increasing the strength of these particle-particle interactions. Pearl chains are typically observed near electrode edges where the strength of the electric field is the greatest. Pearl chains of nanoparticles can be arranged and fused together to create a nanowire or other similar structures. Since the electric field is maximum at the electrode tips and the electric field is minimum away from the electrodes, whether the particle is attracted towards or directed away from the electrodes depends on the relative magnitude of the dielectric constant of the particle, ε_p versus that of the medium, ε_m. Negative dielectrophoresis has the advantage in practice that it allows the collection of particles in a contactless fashion, away from the electrodes and boundaries. Dielectrophoresis offers the controllable, selective and accurate manipulation of the target particles. Based on the discussions above, it is clear that the dielectric forces on the particles depends on the strength and distribution of the electric field, frequency of applied voltage, particle volume and particle and medium dielectric property [29-31]. By controlling the strength and frequency of the external field, it is possible to tune the dielectric forces on particles, or even switch between positive and negative

dielectrophoresis during a single experiment [32-33]. Dielectrophoresis, therefore, is a very versatile engineering tool.

Mixing occurs in many natural phenomena, including geophysical, ocean, and atmospheric flows, and is also an important step in industrial processes involving chemical reactions, fermentation reactions, combustion, and so forth. Traditionally, industrial mixing applications have always been performed using large-scale apparatus. However, in recent years, microscale devices (commonly referred to as microfluidic devices) have been proposed as a means of constructing micro-total analysis systems (m-TAS) and lab-on-a-chip (LOC) devices. However, achieving rapid and efficient mixing of different reactants when performing chemical and biological analyses in such micro fluidic devices is highly challenging [34-37]. Therefore, the problem of developing enhanced micro mixing schemes that are suitable for microfluidic applications has attracted significant interest within industrial and academic circles in recent years. In the present work, efforts have also been made to develop monolayer of dual particulate system model having different polarizability on air-liquid interface under AC electric field.

1.3 Surface Science and Assembly

Self-assembly is a fundamental mechanism by which various structures are formed from the spatial arrangement of atoms, molecules, macromolecules and colloidal particles. It is known that substances can have vastly different properties depending on the way their building blocks are arranged [38-39]. Particles self-assemble on surfaces by design or accident. As compared to immediate continuous interfaces such as liquid or gas phase,

diffusing particles, with distinguishable unique properties such as dielectric constant and or magnetic susceptibility, acquire a dipole moment in a homogeneous external electric (magnetic) field [38-39]. The resulting dipolar interactions can lead to assembly/aggregation of the particles depending on the properties of particles and fluids. During the last few decades, building blocks of desired size, shape and functionality have been engineered at the nanometer and micrometer scales. Various new synthesis and fabrication techniques have been a major focus of interest to academia and industry to not only study orientation and self-assembly of hard and soft colloidal size particles on a liquid-liquid and liquid-gas interface but also to make these structures permanent. The evolved new building blocks from the spatial arrangement of atoms, molecules and particles of novel materials, self-assembling into unique structures, have been made possible solely by their design. Interdisciplinary approach has been well documented in the literature based on the efforts made towards the development of a significant variety of nanoscale building blocks that are potentially capable of self-assembling into larger and more complex systems.

During the last few decades, the scientific challenge has shifted from making new building blocks to organizing them into one-, two-, and three dimensional (1-D, 2-D, and 3-D) structures by using electrostatic interactions [40-42], external electric fields [43-44], covalent bonding [40, 45], and capillary forces [40, 46-50]. It is mandatory for colloidal particles to acquire control of particle size and position to create arrays of particles that are periodic for any desired application. Natan et. al. [51] first employed the idea of chemical binding to assemble colloidal particles in 2D, and this work was extended by other researchers including Sato et. al. [52], He et. al. [53], and Zheng et. al [54]. Recently,

various researchers have focused on self-assembly of micron and sub-micron sized particles by employing an external field to induce pattern formation in colloid dispersions [53-61]. In order to understand the possible agglomeration/arrangement of such building blocks requires answering the various fundamental questions based on the properties of building blocks, methodology and applications. The answers to these questions lead to the possibility for many interesting discoveries and technologies.

Surface science has been one of the first beneficiaries of self-assembled nanostructures (in the form of Self Assembled Monolayers (SAMs)) [62]. Particles self-assemble on surfaces by design or accident. Depending on the quantity of particles, surface density can be described. As the number of particles increase, the surface becomes denser. The more the number of particles, the surface can be less porous. With smaller number of particles, the surface can be more porous.

While self-assembly is a complex problem, it is generally regarded as the most promising approach for designing and controlling particle assemblies for making devices with different functionalities for various applications [63]. It is a process by which disordered particles build an ordered structure through only local interaction. In self-assembling systems, individual particles move towards a final state. The situation considered here is that the self-assembly process is not operated by human hands or tools or mediation, and the particles themselves determine the assembly process. In this respect, self-assembly is more like a generative process than a fabrication process [62, 64-65]. There are various applications of self-assembly including devices such as sensors to detect chemical and biological molecules where in the self-assembly of nanoparticles can be

useful. In addition, it can also be used in creating computer chips with smaller component sizes, which can allow more computing power to be stored in a chip [66].

1.4 Research Objective

Monolayers are thin films formed by the arrangement of single "rows" of particles in a specific pattern on a substrate [67]. Capillary-based self-assembly has applications for a much wider range of inorganic, organic and soft materials, including biological materials and living cells, than is usually possible in traditional front-ends [66-72]. When a floating object is placed on the air-liquid interface, the interface is distorted, which generates a horizontal force (capillary force) against the sidewall enabling the floating object to move toward or away from the sidewall and it depends on the properties of interfaces and of floating objects and the wettability of the sidewall [73-74].

Despite being a subject with enormous potential, the technological implications of the capillary based self-assembly techniques are far from frivolous and research. Efforts are currently in progress to investigate and understand the way in which particles aggregate at an interface, and are able to control the form of the aggregate as well as the dynamics of its formation [75-78].

The capillary based assembly process has been known to be inferior in terms of being able to self-assemble particle patterns due to the absence of long range order; the lattice is packed and non-adjustable. The successful achievement of close-packed self-assembly of particles has been well documented, although its significant challenge is for academicians and technologists to develop an efficient route to achieve adjustable defect-free non-closed self-assembly of neutral particles [79-81,58,59]. Electric field induced alignment and self-assembly of micron size rods, ellipsoids, cubic particles and spherical

particles have been reported on air-liquid and liquid-liquid interfaces [58-59, 82-85]. In this context, successful efforts have also been made in the development of thin films, in the form of embedded self–assembled monolayers of 63 μm, 45μm and 8 μm size glass particles [86,87]. Assembly of 2.25 μm particles and 480 nm silica particle on liquid – liquid film was shown [100].

Motivated by the good initial results in the successful development of self-assembly technique for micron size particles [86,87], further research efforts have been made in the present study to investigate and propose mechanisms for the efficient and robust development of self-assembly of particles of sizes less than 5 μm as well as sub-micron particles and its solid film formation which is not yet shown. The objective of the first part is to develop different solid films containing particles of size 20 μm, 45 μm and 2.25 μm that are arranged in the desired manner. By preheating, assembly of 480nm size particles on liquid film is shown in this work.

Assembly of two different particles has been shown in the literature [88,89]. Self-assembly of dual particulate system of particles of size larger than 20 μm is studied with different particle size and dielectric constant with different liquid medium [88]. In this thesis, the presented outcomes for dual particle assembly are the extension of the previous work and case shown is for particle size less than 10 μm. Also rapid dual assembly is studied by using less viscous and dielectric fluid.

Electric field assembly of particles adsorbed at the droplet and separation of particles from the mixture has been shown previously [90-94]. Here, three different particles - hollow glass spheres, solid glass particles and glass Polystyrene latex are considered. The assembly of hollow glass spheres, solid glass particles, and Polystyrene

latex particles at pole or equator of a freely suspended single floating silicone oil droplet on immiscible castor oil medium is shown. For each case, crossover frequency [91] was investigated experimentally. Using the concept of dielectrophoresis, hollow glass spheres and solid glass particles are sorted out from the mixture on the silicone oil droplet on castor oil medium. At any initial location, the effect of low frequency on flow is described by considering the case of solid glass particles on the silicone oil droplet suspended on corn oil medium.

Surface science has been one of the first beneficiaries of self-assembled nanostructures (in the form of Self Assembled Monolayers (SAMs)). Particles self-assemble on surfaces by design or accident. Depending on the quantity of particles, surface density can be described. As the number of particles increase, the surface becomes denser. The more the number of particles, the surface can be less porous. With smaller number of particles, the surface can be more porous. Transmission probability [using simulation tools such as COMSOL Multiphysics 5.2] is the clear visualization of Brownian motion and the result of probability of number of particles to move from the inner to the outer region in a given medium [95]. It has been observed in the experiment that Brownian motion increases as particles become smaller. It is important in the present study to explore the importance of Brownian motion and thereby, the computation and visualization of transmission probability by particle based approach along with experimental parameters in the absence of force in order to avoid complexity of the assembly process. Hence, the aim is to compute the transmission probability and highlight the visualization of Brownian motion under the conditions of varying viscosity, particle size and temperature.

CHAPTER 2

FIELD INDUCED ASSEMBLY OF MONODISPERSE PARTICLES

2.1 Overview

The study described here is the assembly of particles having same size and same properties. Capillary force can be useful in making monolayers and assembling the particles. However, monolayer formed by this technique is not uniform; it contains defects and has short range order. AC field induced assembly eliminates all drawbacks which are incorporated with capillary force assembly. In this situation, particles are trapped between two liquid interfaces and AC field is applied along the interface. The goal is to develop the solid film which has particles arranged on its surface and this can be achieved by applying the UV light to top liquid. Freezing is not possible if the chosen top liquid is other than UV curable adhesive. Here, the assembly of different sizes of micron and smaller than 5 μm glass and silica particles is shown. The particles are of the same size and properties and hence dipolar force between them will be repulsive. Hence, when an AC field is applied between the electrodes, particles which are trapped on the interface will move apart from each other and begin to assemble.

2.2 Governing Equations

Blinks et al [96] has first described the floating of the particle phenomena at the equilibrium position as shown in Figure 2.1:

$$F_\gamma + F_p = mg \tag{2.1}$$

mg is the particle weight (m is the particle mass, g is the acceleration due to gravity) acting downwards. The vertical capillary force F_γ is given by equation 2.2:

$$F_\gamma = -2\pi a\gamma \sin\varphi_c \sin(\varphi_c + \theta) \tag{2.2}$$

This is due to the vertical component of the interfacial tension $\gamma \sin(\varphi_c + \theta)$ acting upwords at the contact line with length $2\pi a\gamma \sin \varphi_c$ and the vertical resultant of the hydrostatic pressure distribution around the entire particle, F_p is acting also upward.

$$F_p = \rho_w V_{pw} g + \rho_o V_{po} g - (\rho_w - \rho_o) g z_c A_c \quad (2.3)$$

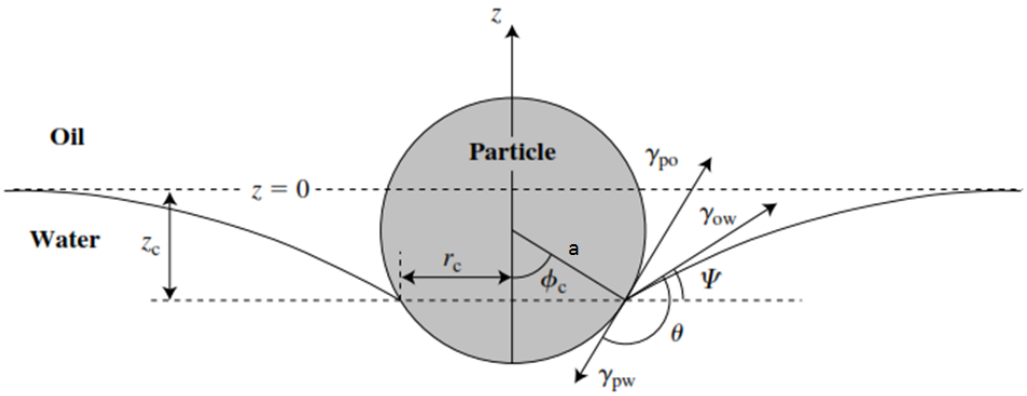

Figure 2.1 Heavy Solid Spherical Particle in equilibrium at Oil-Water Interface. *Source 96*

For a particle floating on a liquid surface, the buoyant weight is balanced by the vertical capillary force.

The force balance equation can be written as:

$$\sin \varphi_c \ \sin(\varphi_c + \theta) = \frac{B}{6}\left[4\,\frac{\rho_p - \rho_o}{\rho_w - \rho_o} - (1 - \cos\varphi_c)^2\ (2 - \cos\varphi_c) + 3\frac{z_c}{a}\ sin^2\varphi_c\right] \quad (2.4)$$

The force balance equation contains one dimensionless parameter, The Bond number (B) $\rho_L a^2 g/\gamma$. Notice that as the particle radius 'a'approaches zero, the Bond number also approaches zero and hence small particles can float without significantly deforming the interface. In equation 2.4, ρ_p, ρ_o, ρ_w is density of particles, oil and water respectively.

It is well known that when a particle is immersed in a fluid and subjected to uniform electric field, it gets polarized but experiences no net force. This is not the case for a particle trapped on an interface. In this case, the particle experiences a force in the direction normal to the interface which varies with a^2 (a is particle radius). The force arises due to the change

in the dielectric constant across the interface. It is necessary to note that the vertical electric force is different from the conventional dielectrophoretic force which varies as a^3. Therefore, the origin of this force is different from the usual dielectrophoretic force. This is important because it means that, for small particles, this force is much stronger than the dielectrophoretic force.

Also notice that if the dielectric constant does not change across the interface, the force will be zero. Adding vertical electric force in force balance equation and considering forces for small particles, the Buoyant weight is the smallest and so the vertical electric force is balanced by the capillary force. Hence there can be considerable interfacial deformation when sufficiently large electric field is applied and so a considerable lateral capillary force makes assembly possible. The electric field also results in lateral dipolar forces which are repulsive and lateral capillary force between the particles which is attractive.

The particle-particle interaction and its assembly can be explained by assuming that the field induces a dipole within each particle. These induced dipoles interact with the external field and also with each other when the particles are very close to each other. When the particles align in chains normal to the direction of the electric field, ‘‘chaining’’ force, F*chain* between adjacent particles [Dipolar force] is given by Velev et al [89, 90, 97-99]:

$$F_{chain} = -C\pi\varepsilon a^2 K^2 E^2 \tag{2.5}$$

Chaining force is dependent on the field strength, E. Here, the coefficient C ranges from 3 to $>10^3$ depending on the distance between the particles and the length of the particle chain [90].

2.3 Material Property and Experimental Setup

Tables 2.1 and 2.2 show the properties of particles and fluids respectively. It is noted that the selection of the particles are based on three main factors. First, their availability in monodisperse form, second, their dielectric property and third, based on their industrial applications. Glass particle has several applications as catalyst, paint and bio-material.

Table 2.1 Properties of Particles-I

Type	**Size**	**Density**	**Dielectric Constant**
Glass Particle(MO-SCI corporation)	20 µm	2.5 g/cm^3	6.9
Glass Particle(MO-SCI corporation)	45 µm	2.5 g/cm^3	6.9
Silica Particles (Cospheric)	2.25 µm	1.8 g/cm^3	6.5
Silica Particles (Cospheric)	480 nm	1.8 g/cm^3	6.5

The work described in this thesis is an assembly of particles on fluid-liquid or liquid-liquid interfaces, and hence the chosen liquids were immiscible with each other. Also, the top fluid is taken to be less dense than the bottom fluid. The fluids are chosen so that the density of top fluid is smaller than the density of the particles so that the particles can easily collect at the interface. In order to cure assembled layer, it is necessary to use top liquid as a UV curable liquid which is taken as an adhesive.

Table 2.2 Properties of Fluids-I

Fluid	Viscosity	Density	Dielectric Constant
Adhesive (Novaguard RTV 800-610)	750 cST	1.1g/cm^3	3.3
Silicone oil (Dow corning FS1265)	3000 cST	1.27 g/cm^3	6.7
Corn Oil Goya	80 cST	0.922 g/cm^3	2.87

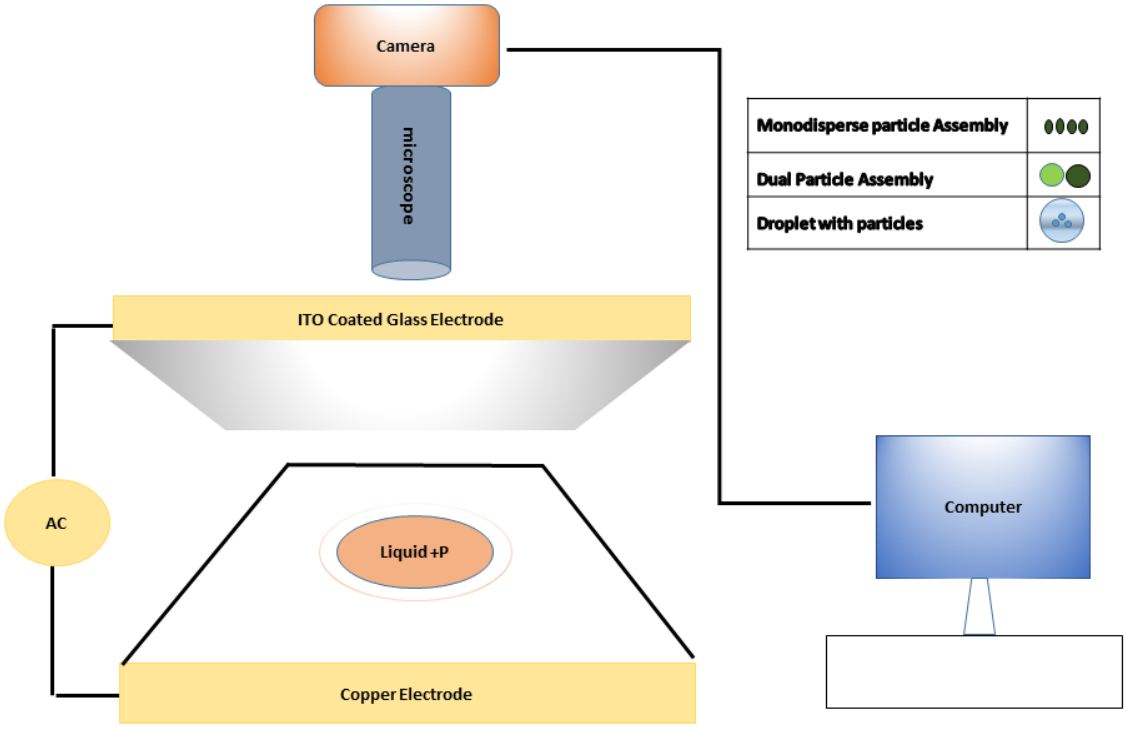

Figure 2.2 Schematic diagram of the experimental setup

Figure 2.2 introduces the schematic diagram of the set up used in the experiment. The unique and important aspect of the setup was a circular chamber for less than 5 µm

size particles and rectangular chamber for larger particles. The height of the chamber was 5.5 mm. Top and bottom part of device were covered with two different electrodes, ITO coated transparent glass electrode (Thin film Device Incorporated, CA) and copper electrodes respectively. The gap between the two electrodes was 6mm. The chamber contained two immiscible fluids placed on top of each other and separated by an interface.

To obtain particle free from moisture and eliminate the chances of cluster, particles were heated before use. After preheating, suspension was made with particles and top liquid and then uniformly mixed by using magnetic stirrer. Depending on the size of the particles and viscosity of the top liquid, particles take time to reach the interface. Small particles take more time to reach the interface. As the viscosity of the fluid increases, reaching time of particles to the interface will increase. Then the device is covered with transparent glass (ITO coated electrode). Hence, the assembly process is observed and/or recorded through a microscope or computer interfaced with microscope (Nikon Eclipse E600). Signal generator (BK Precision Model 4010 A), amplifier (Trek Model 610E) and oscilloscope were used to apply a high electric voltage between the two electrodes. A frequency was set to 100 Hz and electric field was applied along the interface. The maximum applied voltage was 7 kV-10kV depending on the size of the particles. After assembling the particles, UV light was used to cure the top fluid.

2.4 Results and Discussion

The combined action of DEP and electric force can be used as a tool for AC field-driven assembly of particle structures [90]. Here alternating electric fields was applied to the gap between the two electrodes. It is important to note that particles experience DEP force only

in a non-uniform electric field and the DEP force does not depend on the field polarizability. Particle movement in field gradients occurs because the force acting on the two poles is not the same due to the gradient in the field. Particles used in the experiments are monodisperse and have similar properties and hence they have same polarizability. Therefore, when an electric field is applied, repulsive lateral dipolar force causes particles to move away from each other. As particle size decreases, it takes longer time to get arranged because of the increase in Brownian forces. Submicron sized particles are difficult to self- assemble and require a more strong uniform electric field.

2.4.1 Solid Film with Assembled 20μm Glass Particles

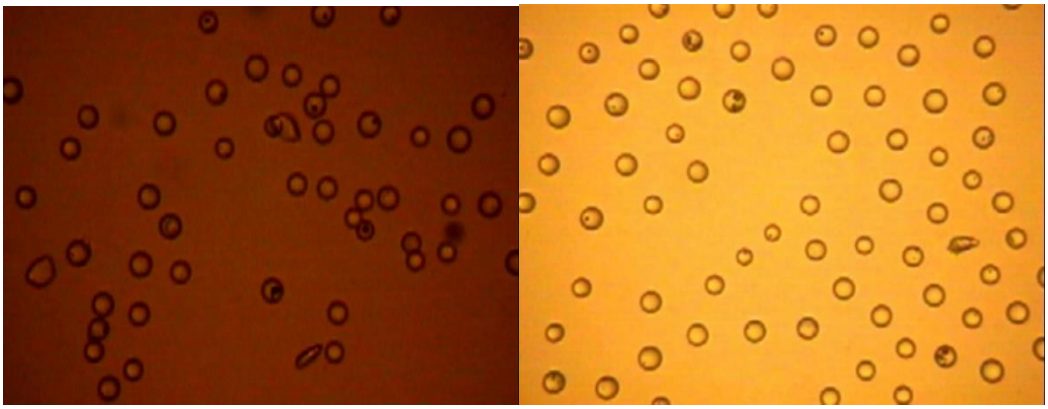

(a) (b)

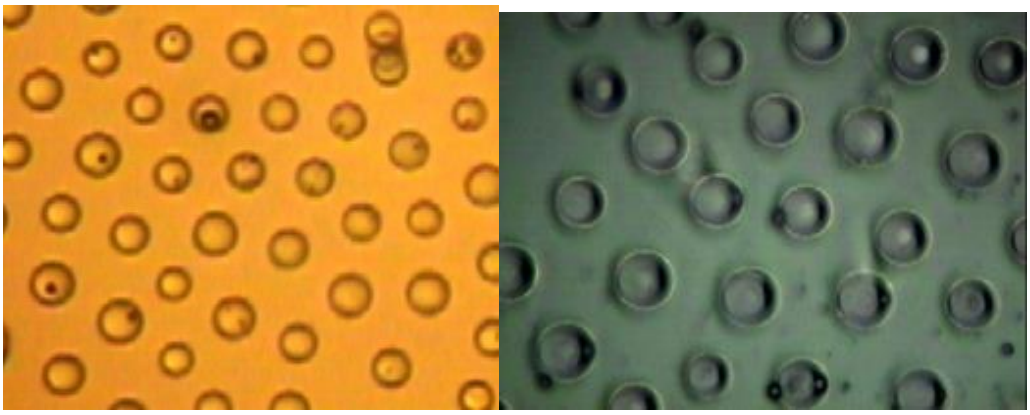

(c) (d)

Figure 2.3 Initial image of 20 μm particles under capillary force 200x magnification (a), Particles are influenced by electric field and start to arrange (b), self-assembled and arranged 20 μm particles on two liquid interfaces before freezing at 200X magnification after electric field is applied (c), Microscopic view of flexible solid film with 20 μm particles after curing/freezing 500X magification (d).

Monolayer of 20 μm particles on two liquid interfaces and on solid film are described in this section. As discussed in the experimental set up, a rectangular device was used and glass particles with 20 μm glass particles were sprinkled on the top liquid after preheating. Particles take almost 30-45 minutes to reach the interface. Top liquid in this case was UV curable adhesive and bottom liquid was silicone oil. Figure 2.3 (a) shows the initial images (before applying the electric field) of 20 μm particles. Initially, particles formed clusters

because of the lateral capillary force. Once the electric field is applied, because of repulsive lateral dipolar force, particles moved away from each other and started to arrange under the influence of the electric field (Fig 2.3 (b)). The monolayer of 20 μm glass particles were arranged and formed monolayer in the interface of two liquids after an electric field is applied. Also they formed long range order as shown in Figure 2.3 (c). Inter-particle spacing is 2*a*. After the field was turned off, the monolayer was cured by applying UV light. The curing time for the resin was less than 60 seconds. The monolayer in the interface between the two fluids became embedded in the surface of the solid thin film. After the film was fully cured, any remaining silicone oil on its surface was rinsed away. In Figure 2.3 (d), a solid thin film with 20 μm particles is viewed under the microscope.

2.4.2 Soild Film with Assembled 45 μm Size Glass Particles

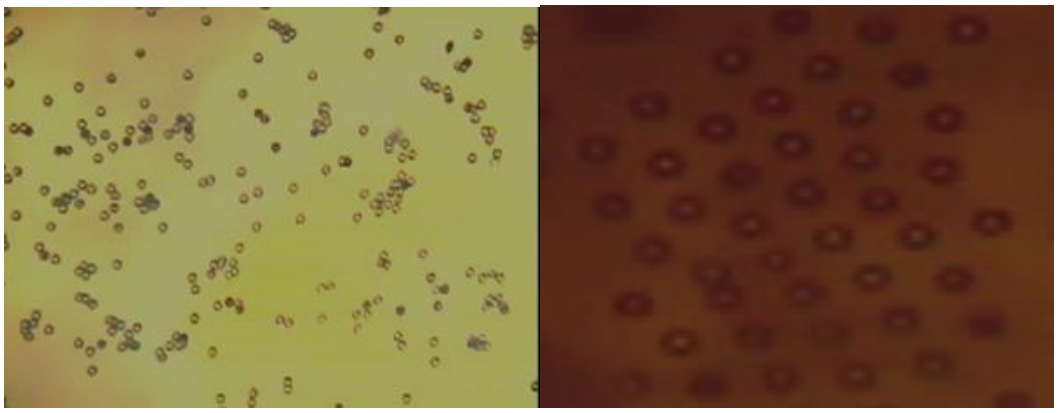

(a) (b)

Figure 2.4 Initial image of 45μm glass particles 50X magnification (a), Arranged 45 μm particles on two liquid interfaces on 200X magnification after electric field applied (b)

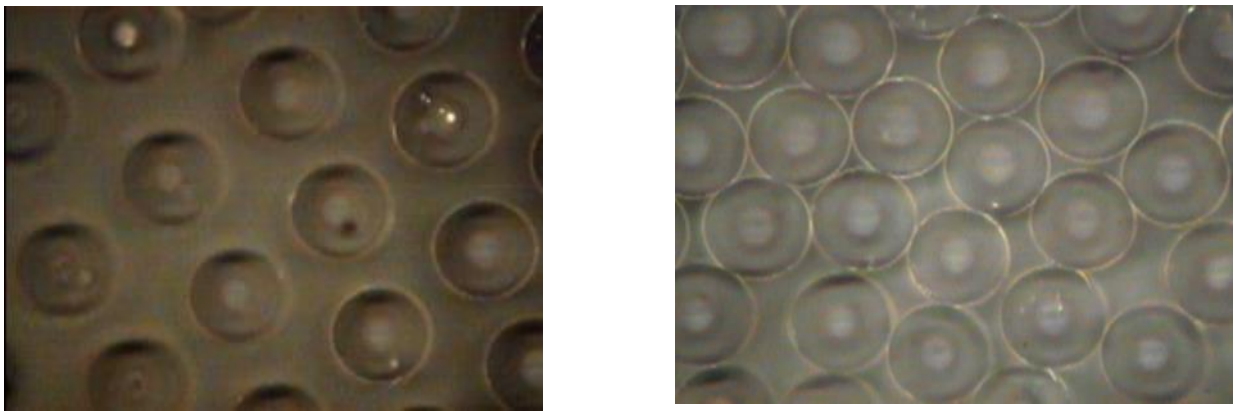

(a) (b)

Figure 2.5 Microscopic view of flexible solid film with 45μm particles after curing/freezing 500X magification (a) and (b)

Here it is noted that work on 45 μm particles has been performed previously [86,87]; the only difference is that the particles are preheated in order to eliminate the moisture and particle concentration. Figure 2.4 (a) is the initial image of the particles which is taken before applying an electric field, Figure 2.4 (b) is taken after the electric field is applied in which it can be seen that the particles got arranged in the interface between two liquids and Figure 2.5 is the microscopic view of solid film after freezing. The inter-particle distance between 45 μm particles, after freezing, is 1*a*.

2.4.3 Assembly of Silica Particles Size Less than 5 μm

For smaller particles, Brownian motion is a vital factor because Brownian motion increases with decrease the particle size. Assembling was more difficult, because their shape and size were more difficult to control. For small particles, buoyant weight is the smallest; so the vertical electric force is balanced by the vertical capillary force. Hence there can be non-negligible interfacial deformation when sufficiently large electric field is applied and a non- negligible lateral capillary force which makes assembly of small particles possible [81-83, 85-87]

2.4.3.1 Development of Solid Film with Assembled 2.25 µm Silica Particles

In an earlier study [100], it was shown that 2.25 µm silica particles self-assembled and arranged under the applied electric field and monolayer was formed between corn oil-adhesive interfaces. However, after several efforts, success was not achieved in making a solid film which has assembled and arranged 2.25 µm particles on its surface; this is a limitation of the present work. The reason for not being succeesful might be the chosen interface, which was selected - the corn oil as top liquid and UV-curable resin as a bottom liquid. Under the influence of UV light, arrangement of particles gets disturbed which results in agglomeration during the curing process (Figure 2.6(a)). The possible reason for agglomeration/cluster is the presence of corn oil as a top fluid which hinders the curing process and results in the stress generation at the interface in the final cured solid film. In order to further evaluate the influence of the UV-curing on the solid film, scanning electron microscopic analysis of the film was carried out which is shown in Figure 2.6 (b).

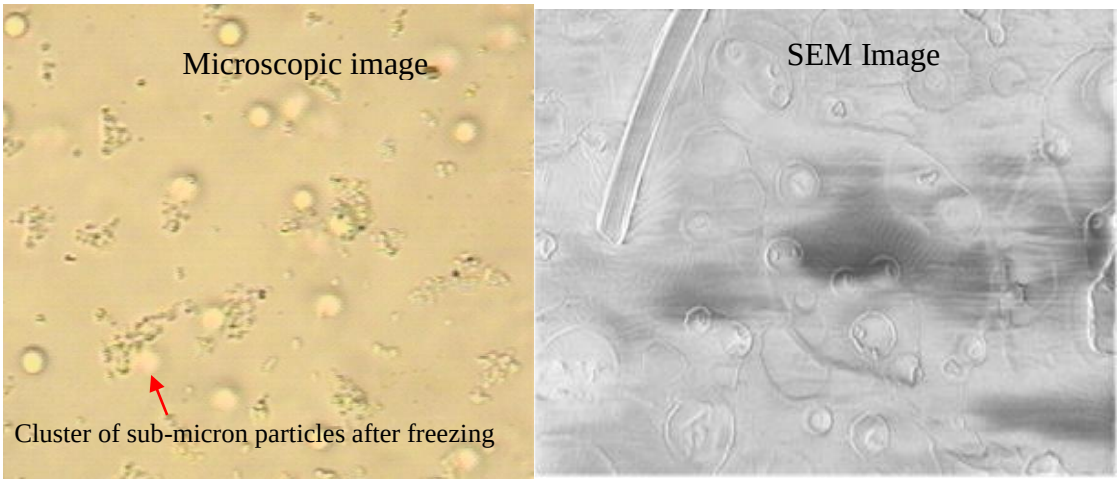

(a) (b)

Figure 2.6 2.25 µm particles on solid film showing that the arrangement got disturbed after freezing (a), Scanning Electron Microscopy (SEM) image of 2.25 µm particles with irregular arrangement on solid film (b).

In order to overcome the above mentioned limitation and to achieve a goal of the present study, systematic efforts are carried out for optimization of various experimental parameters. The interface selected in the present study is UV-curable adhesive as a top fluid and silicone oil as a bottom fluid. The time required to reach the particles at interface would be increased as compared to the earlier study since the adhesive viscosity is ten times higher than that of corn oil. Figure 2.7 (a) shows the initial image of the particles at the interface of two liquids before applying the electric field. Figure 2.7 (b) shows the image of 2.25 μm particles influenced by electric field at the liquid-liquid interface. Because of the selection of top interface as UV curable adhesive, 2.25 μm particles can be assembled, arranged and monolayer can be formed. The monolayer was then cured within 60 second into a solid film as shown in Figure 2.7 (c) after applying UV light and the excess silicone oil was removed. It is feasible to obtain the arrangement of the particles on solid film even after curing/freezing that can be seen in Figure 2.7 (d). The arrangement of particles on the solid film is not disturbed. Inter-particle spacing was 6*a*.

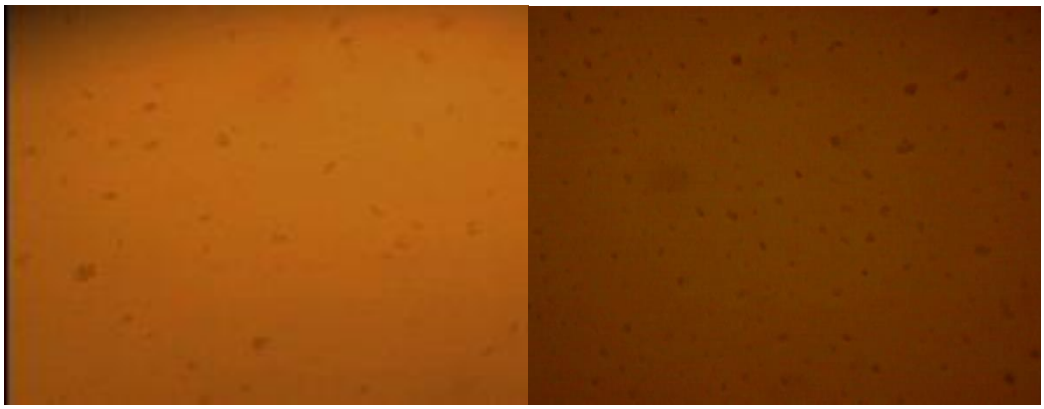

(a) (b)

(c) (d)

Figure 2.7 Initial image of 2.25 μm particle (a), 2.25 μm particles influenced by electric field (b), Solid film of 2.25 μm silica particles after freezing (c), Microscopic view of solid film which has 2.25 μm particles arranged on it (d).

2.4.3.2 Assembly of 480 nm Silica Particles on Corn oil –Adhesive Interface

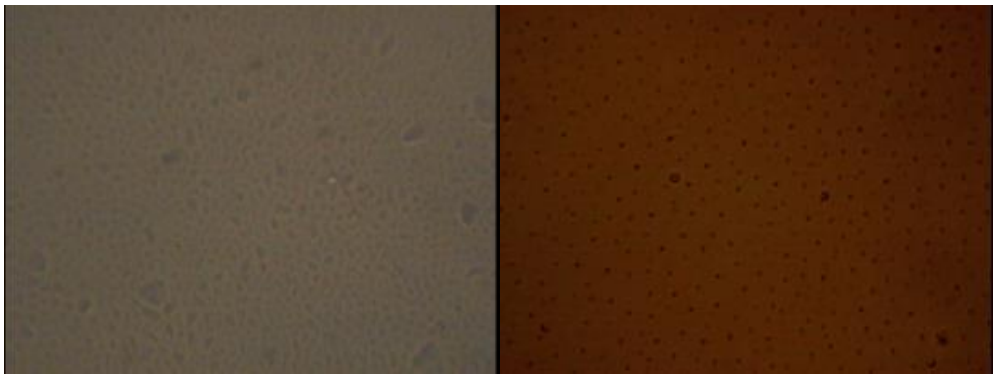

(a) (b)

Figure 2.8 480nm silica particles on 500X magnification before electric field applied on adhesive-corn oil interface (a), arrangement of particles after electric field is applied at 500X magnification (b).

Figure 2.8(a) refers to the image of 480 nm silica particles before electric field is applied. Here it is to be noted that the top liquid is corn oil and the bottom liquid is UV curable adhesive. Because of the very low viscosity of the corn oil, the 480 nm silica particles started to respond to the electric field within a very short time. Figure 2.8(b) shows the arrangement of 480 nm silica particles on the corn oil – UV-curable adhesive interface after the application of a voltage of 7 kV (Peak to valley).

As mentioned in the previous case of 2.25 μm particles, freezing or curing will hinder the arrangement of the particles since corn oil is used as the top fluid. In order to freeze 480 nm silica particles, the interface must be replaced with adhesive and silicone oil.

CHAPTER 3

FIELD INDUCED ASSEMBLY OF DUAL PARTICLES

3.1 Overview

Electric force is capable of assembling layer of particles of two different sizes and different properties on a liquid-air interface which cannot be possible by capillary based technique [88-89]. The pattern formation of dual particles depends on three factors; (1) Relative Size of Particles, (2) Extent of polarizability and (3) Applied Electric Field Intensity. Lateral capillary force between two particles is attractive. Particles can be polarized positively or negatively depending on the dielectric property of particles and interface and extent of polarizability under applied electric field. The dipolar force can be repulsive, when both the particles are positively or negatively polarized and attractive when both particles have different polarizability. In order to exploit the concept of dual particle assembly [89], opposite polarized particle mixtures are studied which form ring structure. Selection of top and bottom fluids, particle sizes and the electric field intensity were additional parameters affecting the intensity of the force [88].

3.2 Governing Equations

When an electric field is applied, the total lateral force between two particles is given by [88]:

F_l= Lateral Capillary force ($\frac{f_i f_j 1}{2\pi\gamma r}$)+ Dipolar force ($\frac{3p_i p_j 1}{4\pi\varepsilon_o\varepsilon_L r^4}$) (3.1)

Here, fi – vertical force acting on the ith particle

f_j – vertical force acting on the j^{th} particle

p_i - induced dipole moment of i^{th} particle

p_j - induced dipole moment of j^{th} particle

γ - interfacial tension

r - distance between the particles

ε_o and ε_L - permittivity of free space and bottom liquid respectively.

Now, the lateral capillary force has two contributions - buoyant weights and the vertical electric forces. Lateral capillary force is attractive which causes particles to come together. Dipolar force is also attractive as particles taken in this study have opposite polarities. As both forces are attractive, particles are in contact with each other. Finally, dual particles form a composite arrangement. In the presence of a strong electric field, the capillary and dipolar forces are stronger than Brownian forces making self-assembly of micron- to nano-sized particles possible [55, 85-87].

3.3 Material Properties

Summary of the properties of particles and fluid, respectively, utilized in the experiments, is presented in Tables 3.1 and 3.2. Same experimental setup was used as described in section 2.3 and shown in Figure 2.2 in order to make assembly of dual particles.

Table 3.1 Properties of Particles-II

Type	Size	Density	Dielectric constant
Glass Particle(MO-SCI corporation)	20 µm	2.5 g/cm^3	6.9
Glass Particle(MO-SCI corporation)	8 µm	2.5 g/cm^3	6.9
Copolymer Particle (Duke Scientific corporation)	71 µm	1 g/cm^3	1
Polystyrene (red Florescent) (Invitrogen 580/605)	4 µm	1 g/cm^3	2

Table 3.2 Properties of Fluid-II

Fluid	Viscosity	Density	Dielectric constant
Adhesive (Novaguard RTV 800-610)	750 cST	1.1g/cm^3	3.3
Silicone oil (Dow corning FS1265)	300 cST	1.27 g/cm^3	6.7
Hallbrite Fluid –BHB	16 cST	0.974 g/cm^3	5.83
Air	14.6 cST	1.165 g/cm^3	1

3.4 Results and Discussion

Referring to Figures 3.1, 3.2 and 3.3, we find that monolayers containing two dissimilar particles, with different dielectric properties, can be assembled by applying an electric field along the interface. In the first case, 71μm copolymer particles and 20μm glass particles were sprinkled on silicone oil. For rapid dual assembly, in the second case, the same particles were sprinkled on very less viscous oil, Hallbrite fluid. In the third case, 8μm glass particles and 4μm polystyrene particles were trapped on air-adhesive interface. Results found that the lateral dipolar force between two particles can be either repulsive or attractive depending on their polarizabilities. The dipolar force between similar particles was repulsive as they have the same polarizabilities, and, therefore, they moved in opposite directions which allowed particles that attracted to come together with particles of opposite polarity resulting in composite particles. Finally, larger particles were surrounded by smaller particles and smaller particles act as a binder. The net force among the particles forming a composite particle was attractive because of the reverse polarities, and so after a composite particle was formed, it remained together until the electric field was turned off.

3.4.1 Ring Structure of 20μm Glass Particles and 71μm Copolymer Latex on the Surface of Silicone Oil

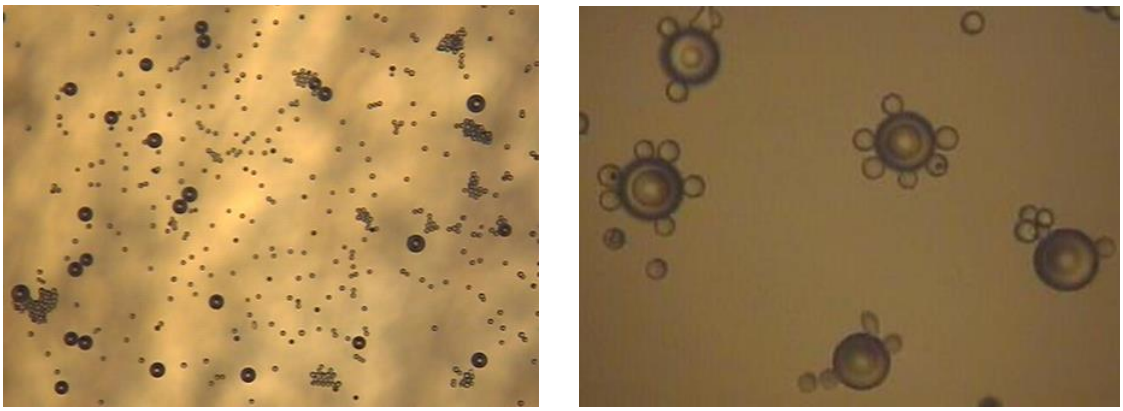

(a) (b)

Figure 3.1. Monolayers of dual particle ring structure of 71μm copolymer and 20μm glass particles on the surface of silicone oil. Initial distribution of both particles magnification 50X (a), After electric field was applied magnification 500X (b) [88].

This is the case when the size of the copolymer particles was almost three times larger than the glass particles and both were sprinkled on to air–silicone oil interface. Initial image of this case is shown on Figure 3.1(a). As mentioned in Table 3.1 and Table 3.2, the dielectric constant of glass particle and silicone oil is 6.9 and 6.7 respectively. This implies that the glass particle has higher dielectric properties than silicone oil (medium) and hence the glass particles are positively polarized in silicone oil. On the other hand, copolymer particles have dielectric constant of 1; therefore, they are negatively polarized in silicone oil. Because of reverse polarity, dipolar force makes glass and copolymer particles to attract when an electric field is applied. Dipolar interaction among glass particles/copolymer particles is repulsive and they move away from each other since they have same polarizability. This is shown in Figure 3.1 (b). The copolymer particles attract the nearby glass particles to form composite particles and form dual arrangement. Results show that the glass particles were surrounded by copolymer particles. Because of the size of the

particles, Brownian forces are negligible; after their adsorption at the interface, the particles do not mix. The particles forming the rings do not touch each other and they interact strongly with the lattice of the glass particles.

3.4.2 Ring Structure of 20μm Glass Particles and 71μm Copolymer Latex on the Surface of Hallbrite Oil

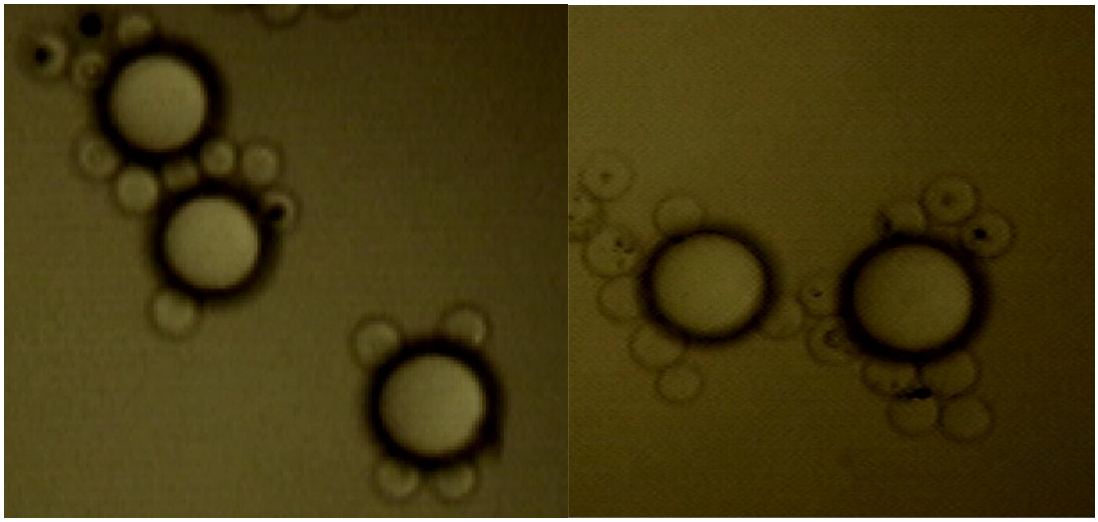

(a) (b)

Figure 3.2. Assembly of dual particle ring structure of 71μm copolymer and 20 μm glass particles on the surface of Hallbrite oil after applying electric field (500X) (a) and (b).

Here the same size of glass and copolymer latex have been used and sprinkled on Hallbrite Fluid. In this case, the dielectric constant of glass particle and Hallbrite fluid is 6.9 and 5.83 respectively. It means that the glass particle has higher dielectric properties than Hallbrite oil (medium) and hence glass particles are positively polarized in Hallbrite. On the other hand, copolymer particles have dielectric constant of 1 and are therefore negatively polarized in Hallbrite fluid. Because of reverse polarity, dipolar force makes glass and copolymer particles to attract when electric field is applied. Dipolar interaction

among glass particles/copolymer particles is repulsive and they move away from each other since they have same polarities. This is shown in Figure 3.2 (a) and (b). The copolymer particles attract the nearby glass particles to form composite particles and form dual arrangement. Result shows that the glass particles are surrounded by copolymer particles. Because of the size of the particles, Brownian forces are negligible and, after their adsorption at the interface, the particles did not mix. It is also observed that the particles respond very fast in Hallbrite liquid compared to silicone oil because Hallbrite fluid has much lower viscosity than silicone oil. Hence, the assembly process consumed less time in Hallbrite liquid compared to silicone oil.

3.4.3 Ring Structure of 8 µm Glass particles and 4 µm Polystyrene Latex

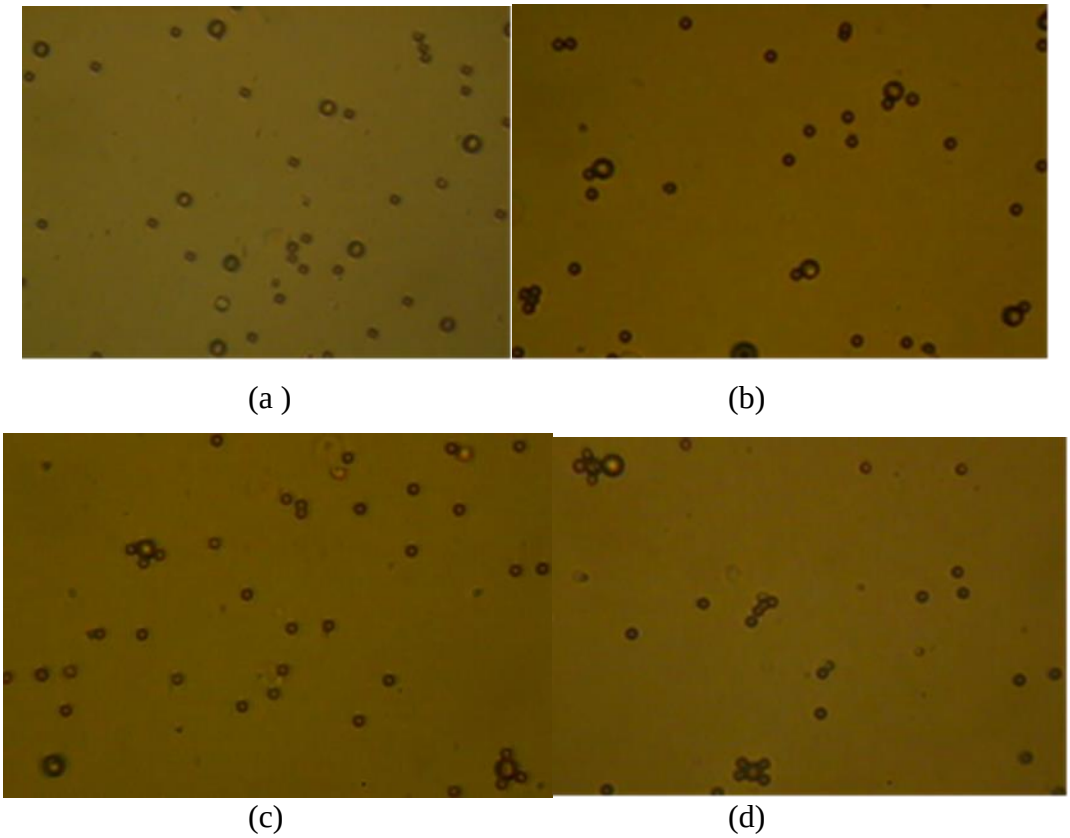

(a) (b)

(c) (d)

Figure 3.3 Assembly of dual particle ring structure of 8µm glass particles and 4µm Polystyrene particle on air – adhesive interface. The magnification is 200X. Initial distribution of both particles (a), After electric field was applied, the mixture self-assembled to form composite particles (b), (c), and (d).

In the second case, Figure 3.3 (a), the glass particles were two times larger than the Polystyrene particles and they were sprinkled on the surface of the adhesive medium. In this case, the dielectric constant of glass particle and adhesive is 6.9 and 3.3 respectively. It means that the glass particle has higher dielectric property than adhesive (medium) and hence the glass particles are positively polarized in the adhesive. On the other hand, Polystyrene particles have dielectric constant of 2; therefore, they are negatively polarized in adhesive medium. Because of reverse polarity, the dipolar force leads to attraction of

glass and Polystyrene particles and they combine together when an electric field is applied. Here Polystyrene particles are surrounded by glass particles. The number of Polystyrene particles which combine with the glass particles increase with time. This means that the longer the electric field is applied, the more polystyrene particles combine with the glass particles - this is shown in Figure 3.3 (b), (c) and (d). In this experiment, particles were used in limited concentration. Use of more number of particles with balanced concentration may give better results.

CHAPTER 4

FIELD INDUCED ASSEMBLY OF PARTICLES ON THE DROPLET

4.1 Overview

In this Chapter, AC field driven assembly of the particles inside the droplet is studied. When an AC electric field is applied at very low frequencies, the electrohydrodynamic flow controls the motion of particles inside the freely single floating droplet. This flow decays with increase in frequency, as shown in a previous study [91]. In this section, the direction of motion of particles is studied in each case experimentally. With values of conductivity of medium and droplet and dielectric properties of medium and particle droplets, Rk factor is calculated [91]. The case described in this study has Rk less than one. Hence, at low frequency, the motion of the particles is from pole to equator. At high frequency, dielectrophoretic force dominates and it depends on the product of Clausius Mossotti factor of particles and droplet liquid $\beta\beta^{'}$ [91-93]. High and low frequency is defined with respect to crossover frequency [90,91]. Crossover frequency is the frequency where EHD and dielectrophoretic force is the same [91]. The applied minimum and maximum frequency are 0.1 Hz and 12 Hz respectively. Clausius– Mossotti factor for droplet and particles are calculated and according to them, the motion of the particles at pole or equator is shown and compared with experimental results. By using this approach, it is possible to assemble the particles at the equator or the pole and sorting out the mixture of two different particles that are adsorbed at the droplet surface [90-94].

4.2 Theoretical Background

The direction of the electrohydrodynamic flow depends on the ratios Rk= R_d/R_m and k = k_d/k_m where R_d and R_m are respectively the resistivity of droplet and liquid medium, while k_d and k_m are the dielectric constants of the droplet and liquid medium [91], respectively.

When Rk> 1, the electrohydrodynamic flow is from equator-to-pole.

When Rk< 1, the electrohydrodynamic flow is from pole-to-equator.

In this study, electrohydrodynamic flow has been exploited experimentally to assemble the particles inside a freely suspended single floating droplet on immiscible medium. Particles collect at the poles when the electrohydrodynamic flow is from equator-to-pole and at the equator when the electrohydrodynamic flow is from pole-to-equator. $\beta(\omega) = \mathrm{Re}(\frac{\varepsilon_d^* - \varepsilon m^*}{\varepsilon_d^* + 2\varepsilon_m^*})$ is the droplet's Clausius–Mossotti factor $\beta'(\omega) = \mathrm{Re}(\frac{\varepsilon_p^* - \varepsilon_m^*}{\varepsilon_p^* + 2\varepsilon_m^*})$ is the particle's Clausius–Mossotti factor with respect to the fluid medium. $\varepsilon_d^*, \varepsilon m^*, \varepsilon_p^*$ are frequency dependent complex permittivity of droplet, medium liquid and particle respectively. The complex permittivity $\varepsilon^* = \varepsilon - j\sigma/\omega$ where ε is the permittivity, σ is the conductivity and $j = \sqrt{-1}$ and E_o is the electric field intensity [90-93].

The DEP force acting on the particles depends on the real part of the Clausius-Mossotti factor. There is a crossover frequency above which the DEP force dominates and below this frequency, the electrohydrodynamic force dominates [91]. It implies that if $\beta\beta' > 0$, the particles assemble at the poles because they are stable at the poles and if $\beta\beta' < 0$, they assemble at the equator where their equilibrium is stable [91]. Table 4.1 shows the calculated values of Rk and $\beta\beta'$

Overall, the particles can be assembled on the pole or equator by determining the correct crossover frequency. Crossover frequency is the frequency where the electrohydrodynamic and DEP forces are equal. Below crossover frequency, frequency is described as low frequency where electrohydrodynamic force dominates the flow direction and frequency above crossover frequency is considered as high frequency where DEP force dominates.

Table 4.1: Calculated Factors for Various Cases

Droplet Liquid	medium Liquid	Particles	Rk	$\beta\beta'$
Silicone oil	Corn oil	Solid glass particles	0.1262	0.091
Silicone oil	Castor oil	Hollow glass spheres	0.1233	-0.044
Silicone oil	Castor oil	Solid glass particles	0.1233	0.018
Silicone oil	Castor oil	Polystyrene latex	0.1233	-0.031

4.3 Material Properties and Methodology

In these experiments, particles mixed with liquid droplets and made dilute suspension. In order to form a droplet with particles, this suspension was injected into the liquid medium by using micro-pipette. Liquids were chosen in such a way that the droplet liquid density is slightly higher than the liquid medium in order to remain as a droplet in a stationary position. AC electric field, with variable frequency in the range of 0.01Hz to 12 Hz, was utilized in this experiment.

Table 4.2 Properties of Particles-III

Type	Size	Density	Dielectric constant
Solid glass particles(MO-SCI. Inc.)	1-3 µm	2.5 g/cm^3	6.9
Hollow glass sphere (Potters industries)	6-32 µm	0.6 g/cm^3	1.2
Polystyrene (red Florescent) (Invitrogen 580/605)	4 µm	1 g/cm^3	2

Table 4.3 Properties of Fluid- III

Fluid	Viscosity	Density	Dielectric constant	Conductivity
Corn oil (Goys Company)	80 cST	0.922 g/cm^3	2.87	20 pS/m
Silicone oil (Dow corning FS1265)	300 cST	1.27 g/cm^3	6.7	370 pS/m
Castor oil (Sigma Aldrich)	750 cST	0.962 g/cm^3	4.7	32 pS/m

4.4 Results and Discussion

4.4.1 Effect of Electrohydrodynamic Force at Very Low Frequency

Here it is experimentally shown that, at any initial location of particles on the droplet, the effect of electrohydrodynamic force decays with increase in frequency. When an AC electric field is applied at low frequency, the motion of the particles is governed by electrohydrodynamic force. Theoretically, the direction of electrohydrodynamic flow depends on the Rk factor. Here, the effect of electrohydrodynamic force at low frequency

was investigated according to the initial location of the particles. The following cases are considered here: case (1). particles are initially concentrated all over the droplet surface; case 2). particles are adsorbed more on pole; case 3). particles are concentrated more on the equator.

Case 1) Particles Initially Adsorbed All Over the Droplet Surface.

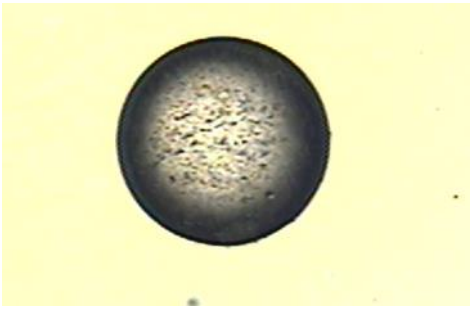

(a)

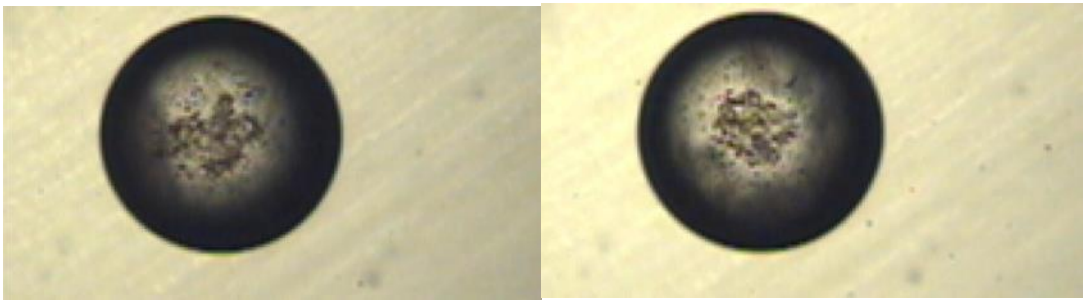

(b) (c)

Figure 4.1. Effect of frequency on Electrohydrodynamic flow of 1-3 μm Solid glass particles Initial Image (a), Droplet at 0.1 Hz frequency (b), Droplet at 0.2 Hz frequency (c).

Figure 4.1(a) is an initial image of 1-3 μm solid glass particles inside the droplet surface. Solid glass particles are denser than liquid drops, silicone oil and liquid medium - corn oil. When an AC electric field is applied, the uniform electric field becomes non-uniform because of the droplet surface. Figure 4.1 b shows that, after a uniform electric

field is applied at 0.1Hz frequency, the particles inside the droplet assemble at its poles. It means that the electrohydrodynamic force is from equator to pole. This flow direction can be towards the pole to equator or equator to pole, depending on the conductivity and dielectric properties of the droplet and liquid medium (depending on Rk). Theoretically, Rk is less than 1 and because of this phenomenon to occur, the particles are pulled from the equator and move towards the pole.

At 0.2 Hz frequency, the amount of particles concentrated on the pole are lesser than the amount of particles concentrated during an applied frequency of 0.1Hz. It means that as the frequency increases, the concentration or growth of particles at the pole decreases. This is clear from Figure 4.1 b) and c). Figure 4.1b has more particles concentrated on the pole as compared to 4.1 c. This is because the electrohydrodynamic flow diminishes with increasing frequency.

Case 2) Particles Adsorbed More On Pole

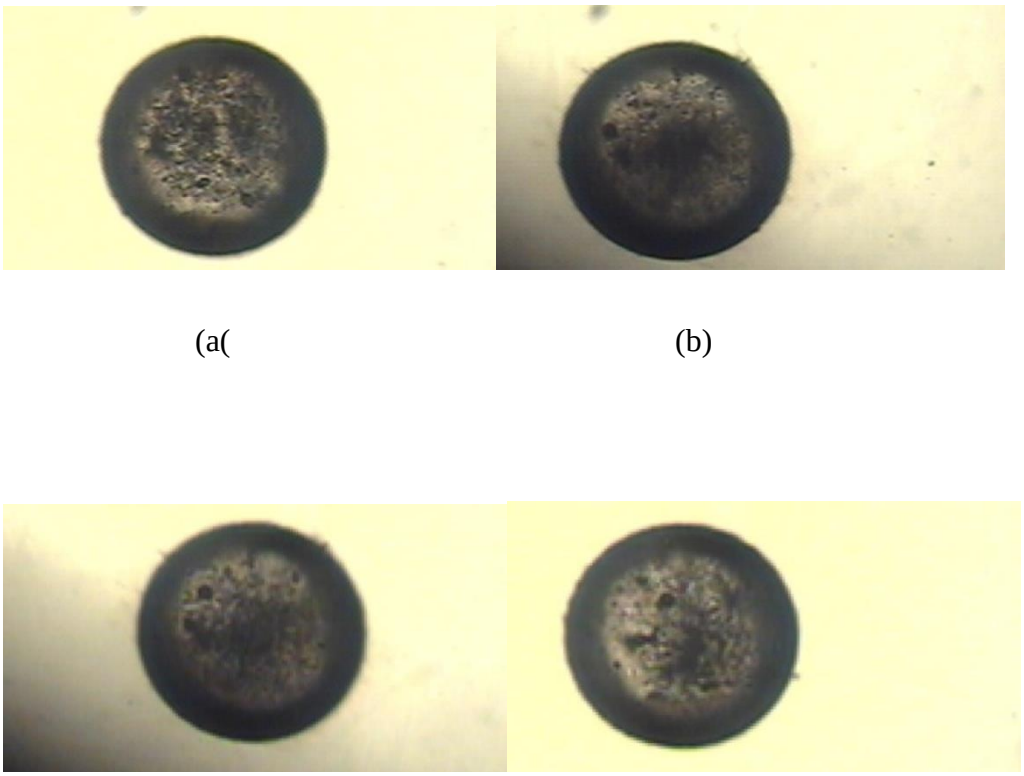

(a((b)

(c) (d)

Figure 4.2. Effect of frequency on Electrohydrodynamic flow of 1-3 μm Solid glass particles Initial Image with particles concentrated at pole (a), Droplet at 1 Hz frequency (b), Droplet at 1.4 Hz frequency (c), and droplet at 1.8Hz frequency (d)

The case when the particles are concentrated more on the pole is shown in Figure 4.2 in which a) is an initial image of the droplet with particles. From Figure 4.2 b) to d), the quantity of the particles which are collected at the pole decreases, as frequency increases. This is because of the decay of the electrohydrodynamic force.

Case 3) Particles Concentrated More On Equator

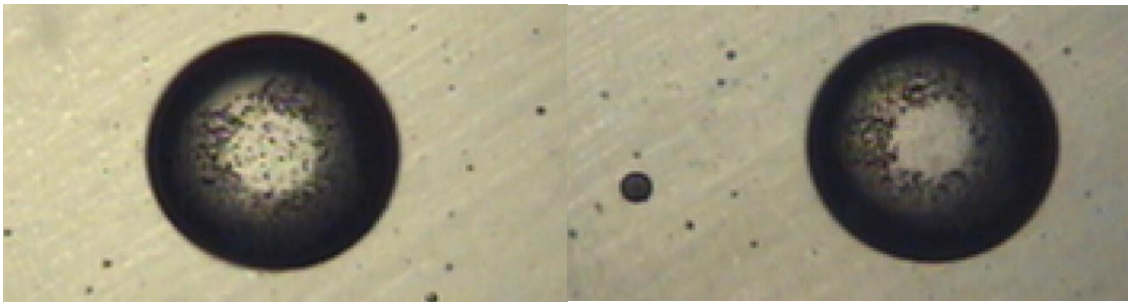

(a) (b)

Figure 4.3 Effect of frequency on Electrohydrodynamic flow of 1-3 μm Solid glass particles droplet at 0.25 Hz (a), Droplet at 0.4 Hz frequency (b)

In the above (Figure 4.3) case, more particles inside a droplet are adsorbed at the equator. The electrohydrodynamic force is more at 0.25Hz frequency. Hence, particles move towards the pole. The effect of electrohydrodynamic force decreases as frequency increases and hence, the amount of particles moving towards the pole is almost negligible at 0.4 Hz.

4.4.2 Assembly Of Particles At Pole Or Equator Of A Droplet:

This is followed by three different cases, where the liquid droplet is silicone oil and liquid medium is castor oil. In the first instance, hollow glass particles were taken into account. Solid glass particles and Polystyrene latex were used in the second and third case respectively. Crossover frequency was investigated experimentally with an applied AC electric field.

Silicone Oil Droplet Contained Hollow Glass Particles On Castor Oil Medium:

This case is shown in a previous study [91], the only difference is particle and liquid concentration. Figure 4.4 (a) is the initial image of silicone oil droplet containing hollow glass particles and the droplet is suspended on castor oil medium. Here, the particle density is lower than that of liquid droplet and liquid medium. Hence, the particles are initially collected at the top surface. Particles, used in this case, are polydisperese hollow glass particles with size varying from 6-18 μm and applied frequency is varied from 0.1Hz to 12 Hz. Hence, the crossover frequency is also varied in this range. At low frequency, the flow of particle is towards the poles and at high frequency, towards the equator. An experimental crossover frequency is found to be at 3 Hz. At frequency of 0.1 Hz, which is below the crossover frequency, the electrohydrodynamic force dominates which tends to move particles towards the pole. This is clear from Figure 4.4(b); it is consistent with the theoretically calculated factor of Rk <1 . Figure 4.4(c) refers to frequency of 6Hz where the particles seem to be at the equator – this is in good agreement with theory since $\beta\beta'$ is negative. At this frequency, the DEP force dominates which tends particles to move towards the equator.

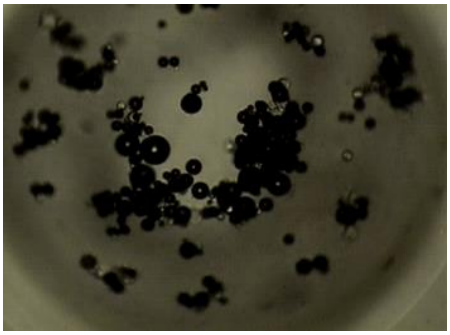

(a)

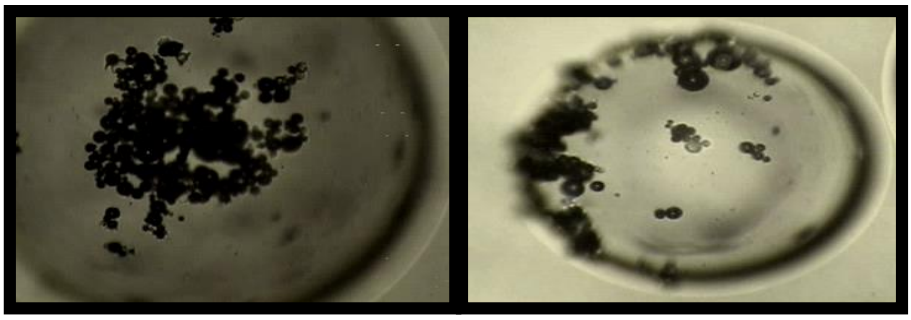

(b) (c)

Figure 4.4 Initial image of silicone oil droplet containing hollow glass particles on the castor oil medium (a), at 0.1Hz particles at pole (b), and at 6 Hz particles at equator (c).

Silicone Oil Droplet Containing Solid Glass Particles On The Castor Oil Medium:

This case is shown in a previous study [91], the only difference is particle and liquid concentration. Figure 4.5 (a) refers to silicone oil droplet containing solid glass particles on castor oil medium where solid glass particles collect at the bottom of the droplet since these particles are denser than the liquid droplet and the liquid medium. It is experimentally determined that, at both low and high frequencies, the particles collect at the poles which are shown in Figure 4.5 (b) and (c) respectively. Experimental results demonstrate that, at low frequency, the flow of particles is controlled by electrohydrodynamic force which pulls particles from equator to pole as Rk < 1 and $\beta\beta'$ is positive; this tends DEP force to move particles to pole at high frequency.

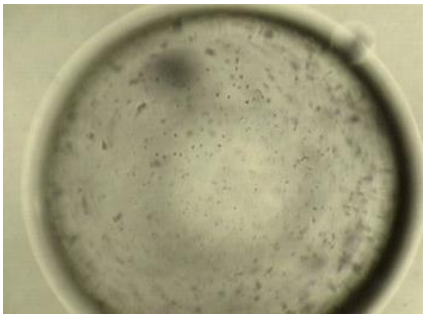

(a)

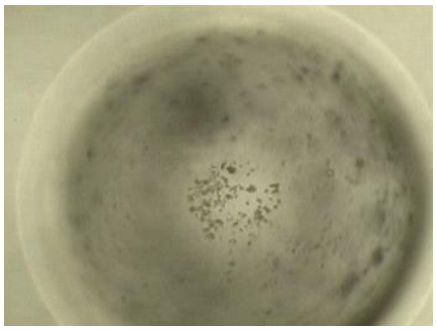

(b) (c)

Figure 4.5 Initial Image of silicone oil droplet containing solid glass particles on the castor oil medium (a), At low frequency, particles at Pole (b) and at high frequency, particles at Pole (c)

Silicone Oil Droplet Containing Polystyrene Latex On Castor Oil Medium:

This case is shown in a previous study [91], the only difference is particle and liquid concentration. Figure 4.6 (a) is the initial image showing the above case. At low frequencies, the electrohydrodynamic flow induced drag dominates and therefore the particles are drawn towards the poles. It is experimentally determined that the crossover frequency is ~ 10 Hz. At 6 Hz frequency, particles collect towards the pole – this is shown in Figure 4.6 (b) and is a good match with theory as Rk < 1. At high frequency, particles move towards the equator because the DEP force dominates. This is shown in Figure 4.6 (c)- it verifies theory because the product of the Clausius-Mossotti factor $\beta\beta'$ is negative.

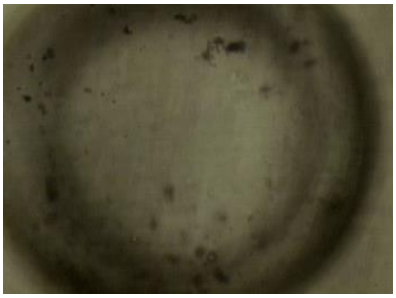

(a)

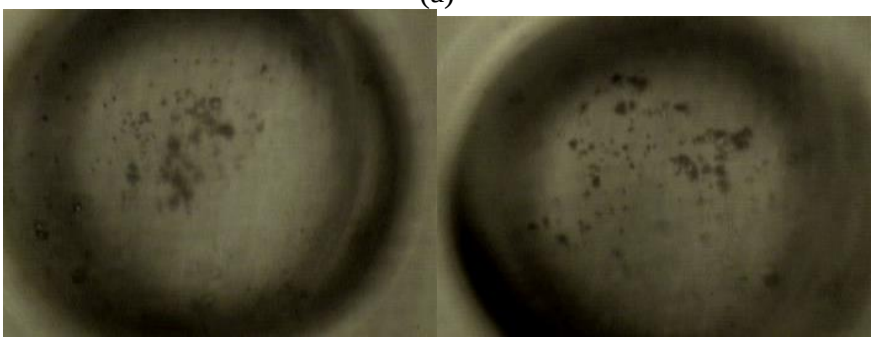

(a) (c)

Figure 4.6 Initial Image of silicone oil droplet containing Polystyrene latex on castor oil medium (a), Particles at Pole at 6 Hz (b), and Particles diverting towards equator at 12 Hz (c)

4.4.3 Sorting Out Hollow Glass Sphere and Solid Glass Particles From Mixture Using Dielectrophoresis

This case is shown in a previous study [91], the only difference is particle and liquid concentration. A mixture of hollow glass spheres and solid spheres inside the freely suspended single floating silicone oil droplet on castor oil medium is taken and shown that the hollow glass spheres and solid glass particles can be separated from the mixture by using dielectrophoresis. As mentioned in Table 4.1, solid glass particles have positive $\beta\beta'$ factor and hollow glass sphere has negative $\beta\beta'$. Hence, solid glass particles experience positive dielectrophoresis and hollow glass spheres are subjected to negative dielectrophoresis. When AC electric field is applied, the solid particles are collected at the area of maximum field intensity and hollow glass sphere move towards minimum area of field intensity. Initial image of mixture of both particles is shown in Figure 4.7 (a). When an AC electric field is applied on the droplet, at low frequencies, both particle types collect at the poles, since the motion of particles at low frequency regime is determined by the

electrohydrodynamic flow and Rk is less than one. At 6 Hz frequency, most of the solid glass particles collect at the poles, and hollow particles collect at the equator which is shown in Figure 4.7 (b).

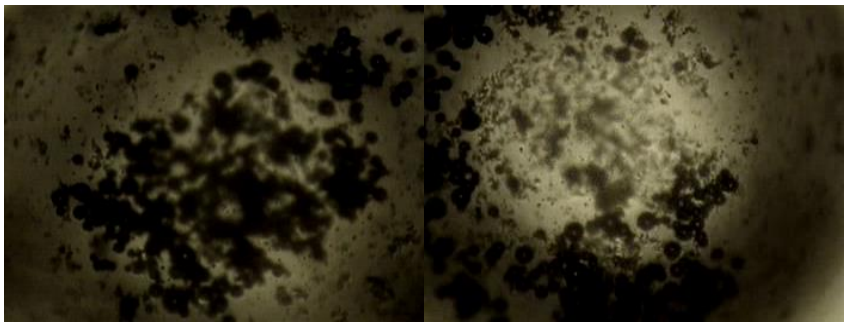

(a) (b)

Figure 4.7 Initial image of mixture of solid glass particles and hollow glass particles (a), Solid glass particles at pole and Hollow glass spheres at Equator at 6Hz (b)

CHAPTER 5

TRANSMISSION PROBABILITY OF DIFFUSING PARTICLES – A CASE STUDY

5.1 Overview

In the present approach, a systematic effort has been made to compute the transmission probability from the inner to the outer domain through COMSOL Multiphysics particle tracing modeling study [95]. The study of diffusion modeling and transmission probability is described by either transport of diluted species or a particle based approach. The diffusion equation is used in transport of diluted species approach whereas, in the particle based approach, Brownian and drag forces result in the diffusion of particles from the inner domain to the outer domain. Transmission probability is an important phenomenon to visualize the Brownian motion and to compute particle diffusion. It is very important to compute the diffusivity for colloidal submicron size particles for varying viscosity, particle size and temperature in order to support the experimental optimization which has not been described till now. The objective in this study is to compute the transmission probability and highlight the visualization of Brownian motion for various viscosity, particle size and temperature.

5.2 Theoretical Background

Particle tracing provides a Langrangian description of a problem by solving ordinary differential equation using Newton's laws of motion. Newton's laws of motion require specification of the particle mass, and all the forces acting on the particle. Considering

Brownian force and drag force in a particle based approach, the equations of motion are as follows [95]:

$$\frac{d(m_p v_p)}{dt} = F_D + F_B \tag{5.1}$$

Drag Force $F_D = \frac{(18\eta)}{(\rho_p {d_p}^2)} m_p (v_f - v_p)$ (5.2)

where, $\frac{(18\eta)}{(\rho_p {d_p}^2)} = \frac{1}{tp}$ (5.3)

tp = particle velocity response time in seconds

Brownian Force $F_B = \lambda \sqrt{\frac{6\pi k_b d_p \eta T}{\Delta t}}$ (5.4)

k_b : Boltzmann Constant

T : *Absolute fluid temperature*

ρ_p : Particle density in kg/m^3

η : *Fluid viscosity*

m_p : Particle mass in kg

v_p : Particle velocity in m/s

v_f : Fluid velocity in m/s

Δt : Time step taken by the solver

d_p : Particle diameter in m

λ : *normally distributed random number*

A different value of λ is created for each particle, at each time step for each component of the Brownian force which leads to spreading of the particles. Transmission Probability from the inner to the outer region is defined as:

$$\text{Transmission Probability} = \frac{\int_o cdS}{\int_I cdS + \int_o cdS} \tag{5.5}$$

where, c is the concentration of particles. I is the inner domain and O is the outer domain.

5.3 Methodology

A detailed experimental setup has been used to carry out the assembly of different types of model particles having varying sizes on air-liquid and liquid-liquid interfaces. The results of these studies have been published elsewhere [55, 85-87, 97]. It has been observed that the optimization of the experimental conditions for the assembly of submicron size particles needs to evaluate in detail the Brownian motion of particles. In the present study, efforts have been made to understand the role of Brownian motion, under the boundary condition validated by the transport of diluted species at the interface and the particle based approach [95]. The governing equation for the concentration of particles is given by [95]:

$$\frac{\partial c}{\partial t} + \nabla.(-D\nabla c) = 0 \tag{5.6}$$

with the initial condition given by a delta function at (0,0): $c_0 = \delta(0,0)$. The initial delta function begins to diffuse from (0,0) radially outwards in all directions. After 100 seconds, some initial concentration will have diffused from the inner circular domain to the outer domain. The number of particles is assumed to be 5000 which are released at the point (0,0) with the initial velocity of all components = zero. The radii of the outer and inner domain are taken as 500 μm and 250 μm respectively. Particles considered in this diffusion model, with density of 2.5 g/cm^3, are dispersed at room temperature in less viscous liquid.

5.4 Results and Discussion

In this study, efforts have been made to compute the transmission probability through a particle-based approach for 2.25 and 0.480 μm solid glass particles as a model system. This transmission probability represents the diffusivity of the model system. Also, the Brownian motion of the particles in a fluid is the key parameter to investigate and can be visualized under the influence of the properties of particles and fluids. By using the COMSOL Multiphysics module [95], simulations have been performed with particle based approach and the transmission probability has been computed as function of viscosity, particle size and temperature. In this particle based approach, Brownian and drag force are added which are stochastic [101-103] and, therefore, it was required to solve the problem multiple times and a statistical average of the results is obtained.

Particle Tracing of 2.25 μm Silica Particle

The computation of transmission probability can be carried out with two different methods. First is the transport of diluted species at the interface and the second is the particle based approach. The number of particles is assumed to be 5000 which are released at the point (0,0) with initial velocity of all components is zero. The radii of the outer and inner domain are considered to be 500 μm and 250 μm respectively. The particles, considered in this diffusion model, are 2.25 μm silica particles with density of 2.5 g/cm^3, dispersed at room temperature, in less viscous liquid. The transmission probability from the inner to the outer domain is computed by counting the number of particles in the outer domain and dividing it by the total number of particles. This is the main quantity of interest in a particle tracing model.

Transport of Diluted Species In the first method, particles begin to diffuse from (0,0) radially outwards in all directions. After 100 seconds, some of the initial concentration has diffused from the inner region to the outer region. The transmission probability computed by transport of diluted species is 0.2005.

Particle Based Approach In a particle based approach, the combination of drag force and Brownian forces results in the diffusion of particles from regions of high to low number density. In particle tracing, for fluid flow interface, the Brownian and drag force features potentially include random contribution. Because of these features that are included in the model, it is necessary to solve the problem multiple times and take the statistical average of the results. Each time the model is solved, a new set of random numbers is created for each particle, at each time step, which is used to compute the force. The Brownian force feature has a parameter called the additional input argument to the random number generator. In this case, the problem is solved 5 times and for each run, the Transmission probability is computed to be 0.2022, 0.2148, 0.2080, 0.2074, 0.1988 respectively

In each case above, the transmission probability is slightly different; but in all cases, the results are in accord with those obtained from solving the diffusion by transport of diluted species at the interface.

5.4.1 Transmission Probability and Visualization of Brownian Motion at Various Temperatures

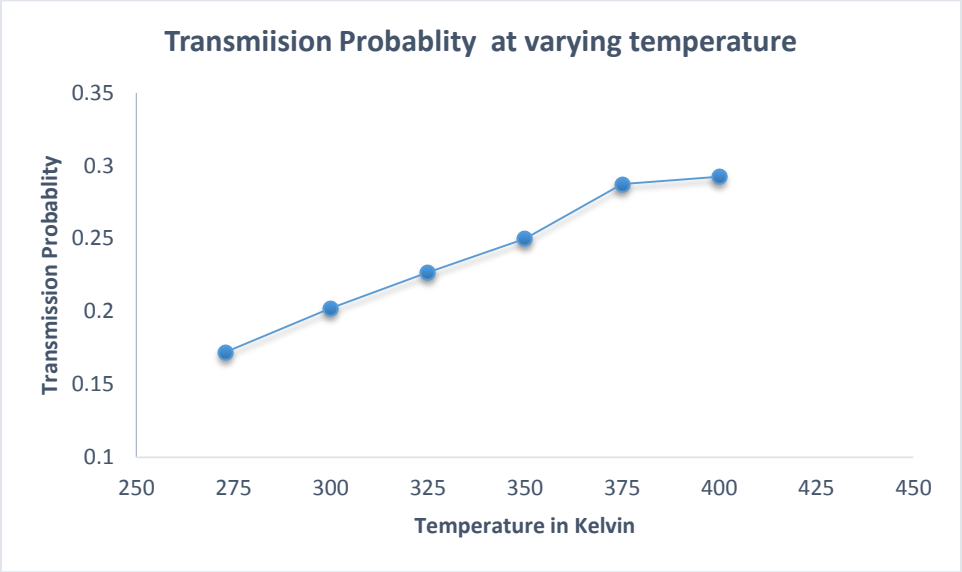

(a)

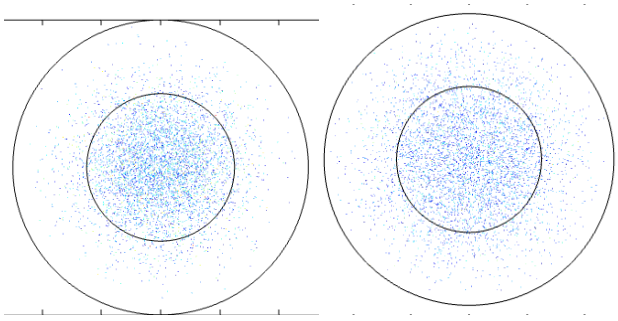

(b) (c)

Figure 5.1 Transmission probability at different temperatures (a), the computed transmission probability 300K (b), and the computed transmission probability at 450K (c)

Figure 5.1 (a) shows the transmission probability with temperature for 2.25 µm silica particles. As temperature increases, more and more particles move towards the outer domain and hence increase the transmission probability and Brownian motion. From the simulation results, shown in Figures 5.1 (b) and (c), the computed transmission probability, at 300 K and 450 K, is 0.2022 and 0.3534 respectively.

5.4.2 Transmission Probability and Visualization of Brownian Motion at Various Viscosity

Figures 5.2 (a) to (d) show the simulated results of transmission probability and the visualization of Brownian motion for 480 nm silica particles at a constant temperature of 300 K for various viscosities. As viscosity deceases, the particle transmission probability increases. At various viscosities, $2x10^{-5}$, $1x10^{-5}$, $0.5\ x10^{-5}$, $0.25\ x10^{-5}$, the particle transmission probability is 0.00318, 0.1868, 0.425, and 0.677, respectively. These results indicate that it is easy for the particles to diffuse in lesser viscous fluid. This implies that it is easy to assemble particles in oil than in water.

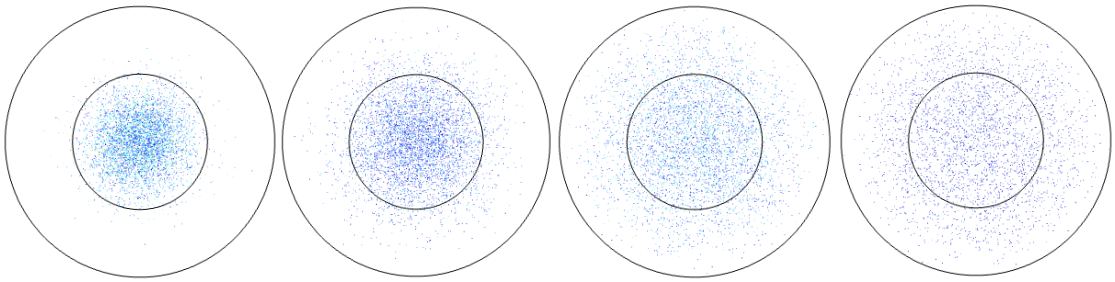

(a) 2E-5 Pa.s (b) 1E-5 Pa.s (c) 0.5E-5 Pa.s (d) 0.25E-5 Pa.s

Figure 5.2 Transmission probability at varying viscosity

5.4.3 Transmission Probability and Visualization of Brownian Motion for Various Particle Size

Figures 5.3 (a) to (d) show the transmission probability and visualization of Brownian motion for different sizes of silica particles which were used in the self-assembly experiment. Particle sizes such as 0.480 µm, 2.25 µm, 8 µm and 20 µm are considered in this simulation. Final location of particles, after 100 seconds, at room temperature in liquid, having the same viscosity, is shown here. With increase in size of the particles, the transmission probability and Brownian motion decreases. This implies that the movement

of the particles towards the outer domain may decrease and less number of particles may transfer from the inner region to the outer domain.

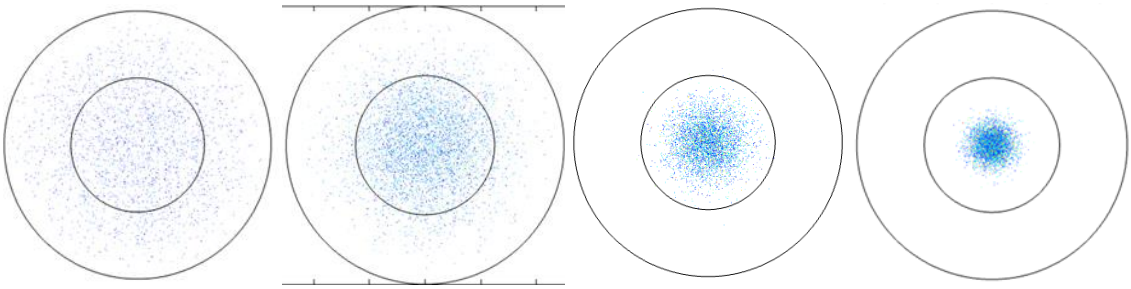

a) 0.480 µm (b) 2.25 µm (c) 8 µm (d) 20 µm

Figure 5.3 Transmission Probability at varying particle size

The results also indicate that the submicron sized particles exhibit more Brownian motion than micron size particles. The transmission probability for particle size of 0.480 µm, 2.25 µm, 8 µm and 20 µm is 0.512, 0.20, 0.00315, and 0 respectively.

Transmission probability and Stokes-Einstein Equation

By utilizing COMSOL Multiphysics module [95], simulations have been carried out with particle based approach and the transmission probability, at different viscosity, particle size and temperature, has been computed. Transmission probability increases with decrease in viscosity and particle size and increases with temperature which is in accord with the Stokes-Einstein equation:

$$D = \frac{k_B T}{6\pi\eta r} \tag{5.7}$$

The above equation relates the diffusion D of a microscopic particle of radius r, undergoing Brownian motion, to the viscosity η of fluid in which it is immersed. This equation is the basis for the theoretical derivation of Fick's laws of diffusion from the consideration of Brownian motion of colloidal particles. These results also lead to the visualization of Brownian motion for different conditions and are in accord with experimental results. [104]

Transmission Probability and Fang and Ning's Results

The presented simulation results of transmission probabilities (with viscosity, particle size and temperature) are in accord with the experimental results of Fang and Ning [105]. In this work, a novel theoretical model of the transport process of micro-particles has been established. Fang and Ning [105] have described and shown that the transport coefficient is a function of the diameter of the micro-particles, density of the fluid, viscosity and temperature. Results in Figure 5.3 show that the transmission probability is inversely proportional to the particle size. This result is supported by the conclusion of Fang and Ning which indicates that the transport of smaller particles is more extended than the larger ones.

CHAPTER 6

CONCLUSION

1. AC electric field induced assembly of regular particles provides important insight into the arrangement of micron and sub-micron sized glass and silica particles on liquid-liquid interface. But, the successful formation of solid film with assembled and arranged particles of size less than 5 μm needs additional understanding. Efforts on the modification of the experimental parameters was described and discussed in the present work. Some success has been achieved in the development of solid film of assembled 2.25 μm silica particles by selecting suitable fluids and altering the interface for the ease of curing process in order to obtain defect free solid films.
2. It is observed that smaller particles (less than 5 μm) take more time to assemble as compared to larger particles (20 μm or more) as they are influenced by Brownian motion. Also particles take more time to reach the interface because of the highly viscous top UV curable liquid.
3. By using AC electric field, particles having dissimilar size and dielectric properties (less than 10 μm) can be assembled and dual particle ring structures can be formed on air-liquid interface. Dual particle ring structure is very fast and rapid on the surface of Hallbrite fluid as compared to silicone oil because of very low viscosity of Hallbrite fluid. Overall, in all cases, smaller particles provide binding to larger particles.
4. AC field induced assembly of the particles at the pole or equator of single floating droplet on immiscible liquid is shown. Experimental results indicate that as frequency increases, electrohydrodynamic flow diminishes and this flow is independent of the

initial location of the particle. By using dielectrophoresis, hollow glass sphere and solid glass particles are sorted out from the mixture inside the droplet.

5. It can be seen that the transmission probability described in this thesis is a function of particle size, temperature and liquid viscosity. From the computation of transmission probability and its findings, clear visualization of Brownian motion for various particle size, temperature and viscosity is obtained. Computation of transmission probability can be useful in surface science where surface density and porosity are applied.

CHAPTER 7

APPLICATIONS

1) An assembly of silica and plastic particle is useful in 2D photonic crystals [90]. Besides this, AC field driven assembly has applications in the formation of electrically functional structures which can be useful in making chemical sensors and bioelectronics circuits. It can be applied in forming microscopic electronic readable biosensors, bioassays, fabrication of nanostructures and DNA detecting probes [106-114]
2) AC field of dual particle assembly is useful in producing biodevices and biomaterials with a high level of functionality, which cannot be produced by conventional techniques [90].
3) Droplet engineering is useful in developing microbioassays [106]. Dielectrophoresis is useful in sorting, transporting and assembling live cells and DNA. It is also useful in separating metallic CNTs and semiconducting CNTs from the mixture [115-117].

   Overall, AC field driven assembly is demonstrated to be more beneficial, convenient and straight forward to implement and control.

CHAPTER 8

SCOPE OF FUTURE WORK

1) In the present work, dual particle assembly is studied on air-liquid interface. The study should be extended to investigate this objective on liquid-liquid interface. Also, the study of dual particle assembly should be explored with live cell-particles.

2) AC field driven assembly, described in this thesis, should apply to conductive particles such as gold, copper and other metals which can be used in microelectronics, drug delivery and several other applications.

3) This study can be applied to anisotropic particles, Janus particles, and live cells.

4) Future experiments should be done with variables such as frequency concentration of liquid and particle suspension, particle type, dielectric constant and viscosity of the surrounding media.

5) Assembly of 480 nm Silica particles on liquid-liquid interface is shown in the present work. Formed assembled monolayer cannot be cured as top fluid is taken a Corn oil. In order to form solid film of assembled layer of 480 nm particles, alteration of interface is suggested. Top liquid should use UV curable adhesive. Hence, the goal to develop solid film of assembled monolayer of 480nm particles can be achieved.

6) Because of the highly viscous top liquid which is UV curable resin, smaller particles take long time to reach the interface and form monolayer. Low viscous UV curable resin is more applicable and practical in order to reduce the time to form monolayer.

REFERENCES

1. Li, F., Josephson, D. P., Stein, A. (2011). Colloidal assembly: the road from particles to colloidal molecules and crystals. *Angew Chem Int Ed Engi, 50 (2),* 360-388.

2. Chang, C.H., Tian, L., Hesse, W., Gao, H., Choi, H. J., Siddiqui, M., Barbastathis, G. (2011). From two-dimensional colloidal self-assembly to three dimensional nanolithography, *Nano Letters, 2011, 11 (6),* 2533–2537.

3. Park, K.C., Choi, H.J., Chang, C. H., Cohen, R. E., McKinley, G. H., Barbastathis, G. (2012). Nanotextured Silica Surfaces with robust superhydrophobicity and omnidirectional broadband super transmissivity. *ACS Nano, 6 (5),* 3789–3799.

4. Ozin, G. A. & Yang, S. M. (2001). The race for the photonic chip: colloidal crystal assembly in silicon wafers. *Advanced Functional Materials 11(2),* 95-104.

5. Subramanian, G., Manoharan, V. N., Thorne, J. D., Pine, D. J. (1999). Ordered macroporous materials by colloidal assembly: a possible route to photonic bandgap materials. *Advanced Materials 11(15),* 1261-1265.

6. J. Gregory, J. (1981). Approximate expressions for retarded van der waals interaction. *J Colloidal Interface. Sci 83(1),* 138-145.

7. Rodnar, S (2002). Interfacial colloidal particle films and their structure formation", PhD thesis, KTH University, Sweden

8. Israelachvili, J (1992). Intermolecular and surface forces, Academic press, San Diego, University of California, Santa Barbara. 3rd Edition.

9. Nunes J. (2010) Controlled Manipulation of Engineered Colloidal Particles, University of North Carolina at Chapel Hill.

10. Ashkin, A., Dziedzic, J., Bjorkholm, J., Chu, S. (1986). Observation of a single-beam gradient force optical trap for dielectric particles. *Optics letters 11(5),* 288-290.

11. Bennink, M.L., Scha¨rer, O.D., Kanaar, R., Sogawa, K.S., Schins, J.M., Kanger, J.S., Grooth, G., Greve, J. (1999). Single-molecule manipulation of double-stranded DNA using optical tweezers: interaction studies of DNA with RecA and YOYO-1. *Cytometry 36,* 200-208.

12. Liu, Y. et al. (1995) Evidence for localized cell heating induced by infrared optical tweezers. *Biophysical journal. 68(5),* 2137-2144.

13. Grier, D. G. (2003). A revolution in optical manipulation. *Nature 424(6950),* 810-816.

14. Laurell T., Petersson, F., Nilsson, A. (2007). Chip integrated strategies for acoustic separation and manipulation of cells and particles. *Chemical Society Reviews 36(3),* 492-506.
15. Ding, X. et al. (2012). On-chip manipulation of single microparticles, cells, and organisms using surface acoustic waves. *Proceedings of the National Academy of Sciences 109(28),* 11105-11109.

16. Nilsson, A., Petersson, F., Jönsson, H., Laurell, T. (2004). Acoustic control of suspended particles in micro fluidic chips. *Lab on a Chip 4(2),* 131-135.

17. Bruus, H. (2012). Acoustofluidics 7: The acoustic radiation force on small particles. *Lab on a Chip 12(6),* 1014-1021.

18. Caleap, M., Drinkwater, B. W. (2014). Acoustically trapped colloidal crystals that are reconfigurable in real time. *Proceedings of the National Academy of Sciences 111(17),* 6226-6230.

19. Hames, B. D. (1998) Gel Electrophoresis of Proteins: A Practical Approach. Vol. 197, Oxford University Press.

20. Gangwal, S., Cayre, O. J., Velev, O. D. (2008). Dielectrophoretic assembly of metallo dielectric Janus particles in AC electric fields. *Langmuir. 24(23),* 13312-13320.

21. Pohl, H. A. (1978). Dielectrophoresis: the behavior of neutral matter in non-uniform electric fields. Vol. 80, Cambridge University press Cambridge.

22. Stuart Williams A. C. (2015). Dielectrophoresis Lab-on-Chip Devices D. Li (ed.), Encyclopedia of Microfluidics and Nanofluidics, Springer Science + Business Media New York.

23. Hughes MP (2003). Nanoelectromechanics in engineering and biology. CRC Press, Boca Raton.

24. Rosenthal, A., Taff, B. M., Voldman, J. (2006). Quantitative modeling of dielectrophoretic traps. *Lab Chip, 6,* 508–515.

25. Muller, T., Pfennig, A., Klein, P., Gradl, G., Jager, M, Schnelle, T. (2003). The potential of dielectrophoresis for single-cell experiments. IEEE Eng Med Biol Mag. 22(6), 51–61.
26. Cummings, E.B. (2003). Streaming dielectrophoresis for continuous-flow microfluidic devices. *IEEE Eng Med Biol Mag. 22(6),* 75–84.

27. Chiou, P.Y., Ohta, A.T., Wu, M.C. (2005). Massively parallel manipulation of single cells and microparticles using optical images. *Nature. 436(7049),* 370–372.

28. Jones, T.B., (2001) Liquid dielectrophoresis on the microscale. *J Electrostatics. 51–52,* 290–299.

29. Washizu, M., Kurosawa, O. (1990) Electrostatic manipulation of DNA in microfabricated structures. *IEEE Trans Ind Appl. 26(6),* 1165–1172.

30. Hunt, T. Westervelt, R. (2006). Dielectrophoresis tweezers for single cell manipulation. *Biomedical Microdevices. 8(3),* 227-230.

31. Zhou, H., White, L. R., Tilton, R. D. (2005). Lateral separation of colloids or cells by dielectrophoresis augmented by AC electroosmosis. *Journal of colloid and interface science. 285(1),* 179-191.

32. Pohl H A. (1978) Dielectrophoresis, Cambridge Univ Press, Cambridge, UK.

33. Gangwal, S., Pawar, A., Kretzschmar, I., Velev, O. D. (2010). Programmed assembly of metallo dielectric patchy particles in external AC electric fields. *Soft Matter 6,* 1413-1418.

34. Ristenpart, W., Aksay, I. Saville, D. (2003). Electrically guided assembly of planar superlattices in binary colloidal suspensions. *Physical review letters 90,* 128303.

35. Nguyen, N.T., Wu, Z. (2005) Micro mixers – a review. *J Micromech Microeng 15,* R1–R16.

36. Chang, C.C., Yang, R.J. (2007) Electrokinetic mixing in microfluidic systems. *Microfluid Nanofluid 3,* 2479–2501.

37. Ottino, J.M. (1989). The kinematics of mixing: stretching, chaos, and transport. Cambridge University Press, Cambridge.

38. Glotzer, S.C., Solomon, M.J., Kotov, N.A. (2004), Self-assembly: From nanoscale to microscale colloids. *AIChE Journal, 50(12),* 2978–2985.

39. Park, J., Lu, W. (2008). Self-assembly of functionally gradient nanoparticle structure. *Applied Physics Letters, 93(24),* 243109.

40. Israelachvili, J.N. (2003). Intermolecular and Surface Forces, Second Edition, Amsterdam, Academic Press, 2003, 450.

41. Alivisatos, A.P., Barbara, P.F., Castleman, A.W., Chang, J., Dizon, D.A., Klein, M.L., McLendon, G.L., Miller, J.S., Ratner, M.A., Rossky, P.J., Stupp, S.I.,

Thompson, M.E. (1998).From Molecules to Materials: Current Trends and Future Directions. *Adv. Mater. 10(16),* 1297-1336.

42. Chen, K.M., Jiang, X., Kimerling, L.C., Hammond, P.T. (2000). Selective Self-Organization of Colloids on Patterned Polyelectrolyte Templates. *Langmuir, 16 (20),* 7825-7834.

43. Tien, J. Terfort, A., Whitesides, G.M. (1997). Microfabrication through Electrostatic Self-Assembly. *Langmuir. 13(20),* 5349-5355.

44. Schmitt, J., Machtle, P., Eck, D., Mohwald, H., Helm, C.A. (1999). Preparation and Optical Properties of Colloidal Gold Monolayers. *Langmuir, 15(9),* 3256-3266.

45. Yeh, S., Seul, M., Shraiman, B.I. (1997). Assembly of Ordered Colloidal Aggregates by Electric Field Induced Fluid Flow. *Nature, 386,* 57-59.

46. Trau, M., Saville, D.A., Aksay, I.A. (1996). Field-Induced Layering of Colloidal Crystals. *Science, 272 (5262),* 706- 709.

47. Trau, M., Sankaran, S., Saville, D.A., Aksay, I.A. (1995) Electric-field-induced pattern formation in colloidal dispersions. *Nature, 374 (6521),* 437-439.

48. Hayward, R.C., Saville, D.A., Aksay, I.A. (2002). Electrophoretic assembly of colloidal crystals with optically tunable micropattern. *Nature, 404 (6773),* 56-59.

49. He, H.X., Zhang, H., Li, Q.G., Zhu, T., Li, S.Y.F., Liu, Z.F. (2000). Fabrication of Designed Architectures of Au Nanoparticles on Solid Substrate with Printed Self-Assembled Monolayers as Templates. *Langmuir, 16(8),* 3846-3851.

50. Jiang, P., Bertone, J.F., Hwang, K.S., Colvin, V.L. (1999). Single-Crystal Colloidal Multilayers of Controlled Thickness. *Chem. Mater. 11,* 2132-2140.

51. Freeman, R.G., Grabar, K.C., Allison, K.J., Bright, R.M., Divas, J.A., Guthrie, A.P., Hommer, M.B., Jackson, M.A., Smith, P.C., Walter, D.G., Natan, M.J. (1995). Self-Assembled Metal Colloid Monolayers: An Approach to SERS Substrates. *Science, 267 (5204),* 1629-1632.

52. Sato, T., Hasko, D.G., Ahmed, H.J. (1997). Nanoscale colloidal particles: Monolayer organization and patterning. *J. Vac. Sci. Technol. B, 15,* 45-48.

53. He, X.E., Li, Q.Z., Zhou, Z.Y., Zhang, H., Li, S.F.Y., Liu, Z.F. (2000). Fabrication of Microelectrode Arrays using Microcontact Printing. *Langmuir, 16 (25),* 9683–9686.

54. Zhang, J., Zhu, Z., Chen, H., Liu, Z. (2000). Nanopatterned Assembling of Colloidal Gold Nanoparticles on Silicon. *Langmuir, 16 (10),* 4409-4412.

55. Aubry, N., Singh, P., Janjua, M., Nudurupati, S. (2008). Micro- and nanoparticles self-assembly for virtually defect-free, adjustable monolayers. *Proc. Natl. Acad. Sci. U.S.A. 105(10),* 3711-3714.

56. Chan, D.Y.C., Henry Jr, J.D., White, L.R. (1981). The interaction of colloidal particles collected at fluid interfaces *J. Colloid Interface Sci., 79 (2),* 410-418.

57. Lucassen, J. (1992). Capillary forces between solid particles in fluid interfaces. *Colloids Surf, 65(2-3),* 131–137.

58. Janjua, M., Nudurupati, S., Singh, P., Aubry, N. (2011). Electric field-induced self-assembly of micro and nanoparticles of various shapes at two fluid interface. *Electrophoresis, 32(5),* 518–526.

59. Aubry, N., Singh, P. (2008). Physics underlying controlled self-assembly of micro- and nanoparticles at a two-fluid interface using an electric field. *Phys. Rev. E, 77(5),* 056302.

60. Bowden, N., Terfort, A., Carbeck, J., Whitesides, G.M. (1997). Self-Assembly of Mesoscale Objects into Ordered Two-Dimensional Arrays. *Science, 276(5310),* 233−235.

61. Dushkin, C.D., Nagayama, K., Miwa, T., Kralchevsky, P.A., (1993). Colored multilayers from transparent submicrometer spheres. *Langmuir, 9(12),* 3695-3701.

62. Whitesides, G.M., Grzybowski, B. (2002). Self-assembly at all scales. *Science, 295(5564),* 2418-2421.

63. Jiang, X.C., Zeng, Q.H., Chen C.Y., Yu A.B. (2011). Self-assembly of particles: some thoughts and comments. J of Materials Chemistry, 21, 16797.

64. Yan, L., Huck, W.T.S., and Whitesides, G.M., (2000). Self-Assembled Monolayers (SAMs) and Synthesis of Planar Micro and Nanostructures, Supramolecular Polymers, Ciferri, A., Eds., Marcel Dekker.

65. Bowden, N., Oliver, S., Whitesides, G.M. (2000). Mesoscale Self-Assembly: Capillary Bonds and Negative Menisci. *J. Phys. Chem. B, 104,* 2714-2724.

66. Wolf, T.D., Holvoet, T. (2005). Emergence versus Self-Organization: Different Concepts but Promising When Combined, in Engineering Self Organizing Systems: Methodologies and Applications, Ed. Brueckner, S., Marzo Serugendo, G. D., Karageorgos, A., Nagpal, R. Springer-Verlag, Berlin, Heidelberg, 1–15.

67. Ulman, A., (1996). Formation and Structure of Self-assembled monolayers. *Chemical reviews, 96 (4),* 1533-1554.

68. Binks, B.P. (2002). Particles as surfactants similarities and differences. *Current Opinion in Colloid & Interface Science, 7(1-2),* 21-41.

69. Blanco, A., Chomski, E., Grabtchak, S., Ibisate, M., John, S., Leonard, S.W., Lopez, C., Meseguer, F., Miguez, H., Mondia, J.P., Ozin, G.A., Toader, O., Van Driel, H.M., (2000). Large-scale synthesis of a silicon photonic crystal with a complete three-dimensional bandgap near 1.5 micrometres. *Nature, 405,* 437-440.

70. Gust, D., Moore, T. A., Moore, A. L. (2001). Mimicking Photosynthetic Solar Energy Transduction. *Acc. Chem. Res, 34(1),* 40-48.

71. Tang, Z., Zhang, Z., Wang, Y., Glotzer, S.C., Kotov, N.A. (2006). Self-Assembly of CdTe Nanocrystals into Free-Floating Sheets. *Science, 314(5797),* 274-278.

72. Jiang, P., McFarland, M.J. (2004). Large-Scale Fabrication of Wafer-Size Colloidal Crystals, Macroporous Polymers and Nanocomposites by Spin-Coating. *J. Am. Chem. Soc, 126(42),* 13778-13786.

73. Cox, P. A., Knox, R. B. (1989). Two-Dimensional Pollination in Hydrophilous plants: Convergent evolution in the genera halodule (cymodoceaceae), halophia (hydrocharitaceae), ruppia (reppiaceae), and lepilaena (zannichelliae). *Amer. J. Bot, 76 (2),* 164-175.

74. Cox, P. A. (1988). Hydrophilous pollination. *Annu. Rev. Ecol, Syst, 19,* 261-279.

75. Della, D., Mahadevan, L. (2005). The "Cheerios effect". *Am. J. Phys, 73 (9),* 817-825.

76. Yuan, J., Cho, S. K. (2012). Bio-inspired micro/mini propulsion at air water interface: A review. *J. Mech. Sci. Technol, 26 (12),* 3761-3768.

77. Hu, D. L., Bush, J. W. (2005). Meniscus-climbing insects. *Nature, 437,* 733-736.

78. Hu, D. L., Prakash, M., Chan, B., Bush, J. W. M. (2007). Water-walking devices. *Exp. Fluids, 43,* 769.

79. Yu, Y., Guo, M., Li, X., Zheng, Q. S. (2007). Meniscus-climbing behavior and its minimum free-energy mechanism. *Langmuir, 23 (21),* 10546-10550.

80. Biswas, S., Drzal, L. T. (2009). A novel approach to create a highly ordered monolayer film of graphene nanosheets at the liquid-liquid interface. *Nano Lett, 9 (1),* 167-172.

81. Bowden, N., Arias, F. A., Deng, T., Whitesides, G. M. (2001). Self-assembly of microscale objects at a liquid/liquid interface through lateral capillary forces. *Langmuir, 17 (5),* 1757-1765.

82. Kralchevsky, P. A., Nagayama, K (1994). Capillary forces between colloidal partiles. *Langmuir, (10),* 23-36.

83. Singh, P., Joseph, D.D. and Aubry, N. Dispersion and attraction of particles floating on fluid–liquid surfaces. *Soft Matter, 6(18),* 4310-4325.

84. Danov, K. D., Pouligny, B., Kralchevsky, P. A. (2001). Capillary Forces between colloidal particles in a liquid film: The finite-Miniscus Proble. *Langmuir, 17,* 6599-6609.

85. Janjua, M., Nudurupati, S., Singh, P., Aubry, N., (2009). Electric field induced alignment and self-assembly of rods on fluid–fluid interfaces. *Mechanics Research communications, 36(1),* 55-64.

86. Singh, P., Hossain, M., Dalal, B., Gurupatham, S.K., Fischer, I.S. (2012) Thin films with self-assembled monolayers embedded on their surfaces. *Mechanics Research Communications 45,* 54-57.

87. Hossain, M., Shah, K., Ju, D., Gurupatham, S., Fischer, I.S., Singh, P. (2013). Self-assembly of monolayers of micron sized particles on thin liquid films. *ASME FEDSM, 16271*, V01CT27A002, 5.

88. Singh, P., Hossain, M., Gurupatham, S.K., Shah, K., Amah, E., Ju, D., Janjua, M., Nudurupati, S., Fischer I.S. (2014). Molecular-like hierarchical self-assembly of monolayers of mixtures of particles, *Nature Scientific Reports, 4 (7427).*

89. Bharti, B., Findenegg, G.H., Velev, O.D., (2014) Analysis of the Field-Assisted Permanent assembly of oppositely charged particles, *Langmuir, 30,* 6577-6587.

90. Velev, O.D., Gangwala, S., Petsev, D.N. (2009). Particle-localized AC and DC manipulation and electrokinetics. *Annu. Rep. Prog. Chem., Sect. C, 105*, 213–246.

91. Amah, E., Shah, K., Fischer, I., Singh, P., (2016) Electrohydrodynamic manipulation of particles adsorbed on the surface of a drop. *Soft Matter, 12,* 1663-1673.

92. Nudurupati, S., Janjua, M., Singh, P., Aubry, N. (2010). Concentrating particles on drop surfaces using external electric fields. *Soft Matter, 6*, 1157–1169.

93. Nudurupati, S., Janjua, M., Aubry, N., Singh, P. (2008). Concentrating particles on drop surfaces using external electric fields. *Electrophoresis, 29,* 1164–1172.

94. E. Amah, K. Shah, I. Fischer and P. Singh, Self-assembly and Manipulation of Particles on Drop Surfaces, ASME 2014 4th Joint US-European Fluids Engineering Division Summer Meeting (FEDSM' 14-21792) Chicago, Illinois, August 2014.

95. Brownian Motion, Solved with COMSOL Multiphysics 5.2 (2015).

96. Binks B. P. (2006). Colloidal Particles at Liquid Interfaces" Eds. Binks, B.P., Horozov, T.P., Cambridge Universty Press, Cambring.

97. Velev, O.D., Bhatt, K.H. (2006). On-chip micromanipulation and assembly of colloidal particles by electric fields. *Soft Matter, 2,* 738-750.

98. Velev, O.D., Kaler, E.W. (2000). Structured Porous Materials via Colloidal Crystal Templating: From Inorganic Oxides to Metals. *Adv. Mater, 12(7),* 531-534.

99. Velev, O.D., Kaler, E.W. (1999). In Situ Assembly of Colloidal Particles into Miniaturized Biosensors. *Langmuir, 15(11),* 3693-3698.

100. Singh., P. (2014) System and Method for formation of thin films with self-assembled monolayers embedded on their surfaces, *US20140302312A1*

101. Elliott, R. (1986). Stochastic Calculus Applications, Springer Verlag, Berlin; Mir, Moscow.

102. Borodin, A.N., Salminen, P. (2000). Handbook on Brownian Motion, Birkhäuser Verlag, Basel.

103. Glotzer, S.C., Solomon, M.J., Kotov, N.A. (2004). Self-assembly: From nanoscale to microscale colloids. *AIChE Journal, 50(12),* 2978-2985.

104. Kim, M., Zydney, A.L. (2004). Effect of electrostatic, hydrodynamic, and Brownian forces on particle trajectories and sieving in normal flow filtration. *J. Colloid and Interface Science, 269 (2),* 425-431.

105. Fang H.Y., Ning, M. (2015). Theoretical and experimental studies of the transport process of micro-particles in static water. *Journal of Hydrodynamics, 26(6),* 875-881.

106. v. Rastogi and O. D. Velev, Biomicrofluidics, 2007, 1, 014107–17

107. P. Richetti, J. Prost and P. Barois, J. Phys. Lett. Paris, 1984, 45, 1137–1143.

108. S. R. Yeh, M. Seul and B. I. Shraiman, Nature, 1997, 386, 57–59.

109. C. Faure, N. Decoster and F. Argoul, Eur. Phys. J. B, 1998, 5, 87–97

110. F. Nadal, F. Argoul, P. Hanusse, B. Pouligny and A. Ajdari, Phys. Rev. E, 2002, 65,061409.

111. W. D. Ristenpart, I. A. Aksay and D. A. Saville, Phys. Rev. Lett., 2003, 90, 128303.

112. T. Gong and D. W. M. Marr, Langmuir, 2001, 17, 2301–2304.

113. T. Gong, D. T. Wu and D. W. M. Marr, Langmuir, 2002, 18, 10064–10067

114. O. D. Velev and S. O. Lumsdon, in Handbook of Surfaces and Interfaces of Materials, ed. H. S. Nalwa, Academic Press, San Diego, CA, 2002, pp. 125–163

115. R. Krupke, F. Hennrich, H. von Lohneysen and M. M. Kappes, Science, 2003,301, 344

116. R. Krupke, F. Hennrich, H. B. Weber, M. M. Kappes and H. von Lohneysen, Nano.Lett., 2003, 3, 1019–1023

117. R. Krupke, F. Hennrich, M. M. Kappes and H. V. Lohneysen, Nano Lett., 2004, 4, 1395–1399